RESEARCH ARTICLE

VOLCANICA

Spatio-temporal evolution of the fumarolic field of La Fossa cone (Vulcano Island, Italy) in 2021–2024

Simone Lentini *[α], Marcello Bitetto[β], Luciano Curcio[β], Malte Seefeld[γ], Angelo Vitale[β], Piero Dellino[α], Daniel Müller[δ], Roberto Sulpizio[α], Thomas R. Walter[δ], and Alessandro Aiuppa[β]

[α] Università Aldo Moro di Bari, Dipartimento di Scienze Della Terra e Geoambientali, Bari, Italy.
[β] Università degli Studi di Palermo, Dipartimento di Scienze della Terra e del Mare, Palermo, Italy.
[γ] University of Bonn, Bonn, Germany.
[δ] GFZ German Research Centre for Geosciences, Potsdam, Germany.

Submitted: 2025-04-30 | Accepted: 2025-09-17 | Published: 2025-11-29

Editor: W. Li | Typesetter: G. Seropian

Abstract

Monitoring the spatio-temporal evolution of fumarolic activity is key to understanding volcanic unrest at dormant volcanoes. Here, we present the results of periodic gas surveys conducted at La Fossa (Vulcano Island, Italy) between 2021 and 2024, in which a portable Multi-GAS instrument is used to map the spatial variations in gas composition across the fumarolic field. We identify substantial spatio-temporal changes in gas composition. The crater rim fumaroles exhibit the highest CO_2, SO_2, H_2S, H_2 concentrations and stable, relatively low CO_2/SO_2 ratios (around 20–30), all indicative of a larger magmatic contribution. In contrast, the inner crater fumaroles display more variable and generally higher CO_2/SO_2 ratios, indicating a larger hydrothermal influence. These data, combined with infrared thermal imaging and SO_2 flux results, are indicative of a volcanic unrest that, after having reached its climax in late 2021, has gradually vanished since, although not fully returning to pre-unrest conditions.

Non-technical summary

Hydrothermal fumarolic activity is a common feature of dormant volcanoes worldwide, and its thorough characterization contributes to monitoring and timely detection of volcanic unrest. However, a detailed reconstruction of the anatomy of fumarolic fields, including their spatio-temporal evolution, remains unavailable for many volcano localities. Here, we report on the results of periodic gas measurement surveys conducted at La Fossa, Italy, in 2021–2024, aimed at resolving the spatio-temporal evolution of the fumarolic field. We find a large chemical diversity in the fumarolic field, and we identify and map the areas (the fumaroles on the crater rim) most influenced by deep fluids of magmatic origin. Combined with drone-based thermal imagery and SO_2 flux records, our results are suggestive of a gradual decline of the hydrothermal unrest started in fall 2021. This study corroborates the use of Multi-GAS mapping as a tool for monitoring hydrothermal unrest.

Keywords: Vulcano Island; Geochemical monitoring; Hydrothermal unrest; Volcanic gases; Multi-GAS; Drones.

1 Introduction

The behavior of active volcanoes on Earth is primarily controlled by the rates and mechanisms of magma and gas transport throughout their transcrustal magmatic plumbing system [Cashman et al. 2017; Edmonds and Wallace 2017]. At open-vent volcanoes, mafic magma is efficiently transferred from deeper storage regions to the shallow feeding conduit system to sustain persistent activity, characterized by intense passive degassing and interspersed relatively mild eruptive activity [Edmonds et al. 2022; Vergniolle and Métrich 2022]. Closed-vent volcanoes, in contrast, undergo long-lasting periods of dormancy during which mild fumarolic activity is sustained by degassing of deeply stored, stationary magma. During this background activity, the ascent of magmatic fluids from the magmatic source to surface is limited by the relatively low permeability of rocks/minerals composing the overlying hydrothermal carapace, and is ultimately modulated by spatio-temporal changes in permeability due to variations in the local and regional stress regime [Norton 1984; Chiodini et al. 2022; Marini et al. 2022]. Ultimately, hydrothermal alteration of rocks, and the fluids they host, act as chemical filters [Symonds et al. 2001; Stix and de Moor 2018; Kern et al. 2022] for reactive, water soluble magmatic volatiles (primarily SO_2, H_2S, HCl). Complex gas-water-rock interactions [Giggenbach 1987; 1997; Henley and Fischer 2021] control the chemistry and redox state [Chiodini and Marini 1998; Fischer and Chiodini 2015] of volcanic gases at surface and the physical properties of rocks and associated hazards [Darmawan et al. 2022; Kereszturi et al. 2023].

Because of these intense hydrothermal interactions, closed-conduit volcanoes, during their long inter-eruptive quiescence periods, typically exhibit low temperature fumarolic fields with hydrothermal gas signatures [Giggenbach 1987; Chiodini and Marini 1998]. Typical characteristics include high H_2O/SO_2 ratios (because of dilution of magmatic volatiles by hydrothermal steam; Chiodini et al. [1993]) and high CO_2/S_T ratios (because of preferential sulfur scrubbing by hydrothermal reactions; S_T here stands for total sulfur and corresponds to the sum of SO_2 and H_2S; Aiuppa et al. [2017]). The same fluids also typically have low SO_2/H_2S and CO/CO_2 ratios, and CO_2/CH_4 ratios lower than magmatic gases, because hydrothermal conditions are colder and more reducing than hot,

* simone.lentini@uniba.it

oxidized magma [e.g. Giggenbach 1997; Chiodini and Marini 1998; Chiodini 2009; Oppenheimer et al. 2014; Fischer and Chiodini 2015; Aiuppa and Moussallam 2024]. However, as a volcano becomes restless during unrest, gas composition progressively evolves toward more magmatic compositions (e.g. Turrialba, Vaselli et al. [2010], Kern et al. [2022]), as typically indicated by decreasing H_2O/CO_2 ratios (e.g. Campi Flegrei, Chiodini et al. [2016]; Vulcano, Paonita et al. [2013]), decreasing CO_2/S_T ratios (e.g. Turrialba, Vaselli et al. [2010]), and increasing SO_2/H_2S (e.g. Poás and Turrialba, de Moor et al. [2016], de Moor et al. [2017]), CO/CO_2 (e.g. Campi Flegrei, Chiodini et al. [2012]) and CO_2/CH_4 [Chiodini 2009] ratios. Capturing and interpreting such hydrothermal-to-magmatic transition during volcanic unrest is crucial for volcanic risk mitigation, as it contributes to recognizing when/if the volcanic system is becoming increasingly unstable, and potentially more prone to erupt [Phillipson et al. 2013; Rosi et al. 2022].

To achieve this task, volcanologists mostly rely on performing regular campaigns of direct fumarole sampling [Symonds et al. 1994; Fischer and Chiodini 2015]. However, for large fumarolic systems with many emission vents, direct sampling of all (or even most) fumaroles becomes increasingly impractical and time-consuming, and hence—also to reduce exposure of operators to unsafe, gas-rich environments—the compromise taken is to prioritize sampling of a few key fumarolic targets [Giggenbach 1997]. In such cases, the use of independent methods that allow expedited surveying of the whole fumarolic field becomes a useful complement to direct sampling. This possibility was first opened in the early 2000s by the advent of portable, compact Multi-GAS (Multi-component Gas Analyser System) units [Aiuppa et al. 2005; Shinohara 2005] that allow real-time sensing and measurement of volcanic gas composition. Aiuppa et al. [2005] realized the first walking traverse of the fumarolic field of Vulcano Island in Italy with a hand-held Multi-GAS, operating at 1 Hz and with geo-referenced position given by a co-located GPS. From this, they demonstrated the possibility of mapping the chemical diversity (in terms of CO_2/SO_2 and SO_2/H_2S ratios) of the fumarolic field in circa 1 hour.

The present study builds on previous work by Aiuppa et al. [2005, 2006] and Aiuppa et al. [2022] by reporting on the spatio-temporal variations of the fumarolic CO_2/SO_2 ratio across the Vulcano fumarolic field during 2014 to 2024. We focus on CO_2/SO_2 because, as it has been shown previously at Vulcano [Inguaggiato et al. 2018; Aiuppa et al. 2022] and elsewhere [Aiuppa et al. 2017], this ratio is typically high during periods of reduced hydrothermal activity, when any magmatic sulfur is sequestered by hydrothermal minerals/solutions in the subsurface [Chiodini et al. 1993; Di Liberto et al. 2002]. In contrast, the ratio decreases during phases of unrest when SO_2 escalates faster than CO_2 [Inguaggiato et al. 2022], either because of degassing of mafic magma at depth [Aiuppa et al. 2022] or because of sulfur remobilization from hydrothermal minerals [Chiodini et al. 1993] (or a combination of both). The fumarolic field CO_2/SO_2 ratio serves as a useful tracer to track the alternation of calm and unrest periods that has characterized the activity of La Fossa since the late 1970s [Selva et al. 2020]. Our aim is to reconstruct how the chemistry of the fumarolic field varied in space and time during a period encompassing the autumn 2021 Vulcano degassing unrest [Aiuppa et al. 2022; Di Martino et al. 2022; Inguaggiato et al. 2022; Di Traglia et al. 2023; Inguaggiato et al. 2023; Pailot-Bonnétat et al. 2023; Müller et al. 2024]. We hence extend previous results by describing how the chemical heterogeneity of the fumarolic field evolved after the peak of the unrest was reached in September–December 2021, but has not fully declined yet by time of writing (June 2025).

2 Geological background

2.1 The Aeolian archipelago and Vulcano island

Vulcano is the southernmost island (Figure 1A) of the Aeolian archipelago, an active volcanic arc in the southern Tyrrhenian Sea north of the Sicilian coast, consisting of seven emerged volcanic islands (Stromboli, Panarea, Vulcano, Lipari, Salina, Alicudi and Filicudi) and several submerged seamounts. The Aeolian Islands represent a classic example of volcanic island arc associated with subduction, in this case of the Ionian oceanic crust underneath the accretionary complex south of the Calabrian coast (Figure 1A). The existence of a slab below the arc is confirmed by the distribution of hypocenters along a northwestward subducting plane. The regional tectonics is controlled by the interaction between the spreading Tyrrhenian basins to the north, the subduction of the Ionian slab to the south, and the movements of the Calabro-Peloritan block, mobilized by right lateral strike-slip faults: the Taormina Line (WNW–ESE) until the Middle Pleistocene and then by the Tindari-Letoianni (NNW–SSE) [Mantovani et al. 2023] (Figure 1A). While subaerial volcanic activity started at 1.3 Ma, subaerial volcanism recently concentrated along two axes, Lipari-Salina-Filicudi (270–250 ka) and Stromboli-Panarea-Vulcano-Alicudi (204–106 ka). Erupted magmas range from mafic to silicic, and are calc-alkaline to high-K calc-alkaline series to shoshonitic affinity. Alkaline rocks containing leucite also outcrop at Vulcano (particularly in the Vulcanello area) and Stromboli [Peccerillo 2017].

The geological history of Vulcano alternated phases of (i) construction of volcanic edifices of different size and eruption style, and (ii) caldera collapse events and quiescent phases, characterized by erosion [Keller 1980; Di Traglia et al. 2013; Peccerillo 2017; De Astis et al. 2023]. De Astis et al. [2013] and De Astis et al. [2023] summarizes the evolution of the island in eight eruptive phases beginning by ~130 ka [Soligo et al. 2000; De Astis et al. 2013] (Figure 1B). Between 127 ka and 100 ka, the construction of a shoshonite lava shield (Capo Secco) [Peccerillo 2017] took place, soon covered by a high-K basaltic andesite stratovolcano, known as Vulcano Primordiale that occupied the southern portion of the present island. After an initial caldera collapse (Piano 1) and the emplacement of the Scoglio Conigliara lava flows (99.5 ka), renewed caldera collapse (La Fossa 1) cut the northern section of the previous collapse (78 ka). This event led to the opening of fissures at Timpa del Corvo and Monte Aria, associated lava flows, and the formation of scoria cone at Casa Petrulla [De Astis et al. 2013].

Between 70 ka and 42 ka, after a third caldera collapse cutting through the central portion of the first collapse (Piano 2), new eruptive products were emplaced, mainly from the eruptive fissure at Monte Luccia, as well as from the two scoria cones at Monte Rosso and La Sommata, and from Il Cardo tuff cone (Paleo-La Fossa cone according to De Astis et al. [2013]), which occupied the current location of the La Fossa cone. These deposits covered the previous collapses.

Between 28 ka and 21 ka, a fourth caldera collapse (La Fossa 2) partially affected the northeastern margin of La Fossa, forming the present-day La Fossa caldera. Along its western margins, the Monte Lentia latite to trachy-rhyolite lava domes, flows and pyroclastics were emplaced [Peccerillo 2017], while at the southwestern margins of Piano, the Spiaggia Lunga fissure opened emitting shoshonitic basalt and shoshonite lavas. Additionally, along the southwestern margins of the Piano caldera, the shoshonite to trachyte scoria and pumices of Quadrara fissure formed, accompanied by the Punta Bandiera lava flows to the southeast.

The construction of the La Fossa tuff cone took place between 8 ka to the present [Peccerillo 2017], while the Vulcanello peninsula possibly emerged at circa 2 ka [Di Traglia et al. 2013; Fusillo et al. 2015; Peccerillo 2017; De Astis et al. 2023], or in the Middle Ages [Malaguti et al. 2021]. The most recent estimate of the age of early Vulcanello products is 900–1040 AD [Di Traglia et al. 2024]. Vulcanello is a shoshonite (leucite bearing) to latite lava composite cone with three partially overlapping scoria cones arranged along a NE–SW alignment [De Astis et al. 2013; Di Traglia et al. 2013; Fusillo et al. 2015]. Eventually, by the year 1000, the island of Vulcano became connected to Vulcanello due to activity from La Fossa cone. Compositionally, the La Fossa volcanic successions contain some of the most evolved (trachytic to rhyolitic) rocks on the island, due to a combination of magmatic differentiation and (low extents of) assimilation of upper crust materials of the Calabro-Peloritan Block [Peccerillo 2017]. In contrast, the products of Vulcanello, while sharing some geochemical and isotopic affinity with more evolved La Fossa magmas, represent the most mafic magmas erupted on the island over the last 6000 years [De Astis et al. 2013; Peccerillo 2017].

2.2 The La Fossa tuff cone

The La Fossa tuff cone (Figure 1D) emerges 391 m above sea level on the northern sector of the island. This composite edifice is dominated by a main structure (a tuff cone) rising to an elevation of 251 m, where a sharp slope change separates the crater associated with the Pietre Cotte phase (1731–1775) to the west [De Astis et al. 2013; Di Traglia et al. 2013; Di Traglia et al. 2024] from the post 1775 craters to the east. Several subcircular craters, dating and predating the 1888–1890 eruption [Mercalli and Silvestri 1891], can now be found on the volcano summit (Figure 1D), demonstrating the dynamic and diverse eruptive behaviour over the last millennium.

The eruptive activity at La Fossa cone and associated volcanic sequences have been reconstructed and dated by different authors. De Astis et al. [2013] recognize three main sequences: (i) a lower sequence that includes the Punte Nere and Grotta di Palizzi 1 formations, erupted between ~3550 and 950 BCE [Frazzetta et al. 1984]; (ii) an intermediate portion (Grotta di Palizzi 2 and 3, Carruggi formations and Forgia Vecchia formations), emplaced between ~250 BCE and 776 AD [Keller 1980; Frazzetta et al. 1984]; and (iii) an upper sequence, characterized by the Pietre Cotte and Gran Cratere formations, erupted between 1739 and last eruptive activity occurred in the 1888–1890 eruption [Mercalli and Silvestri 1891].

A different chronology, indicating more frequent eruptive activity in mediaeval time, has been elaborated by Di Traglia et al. [2013], Malaguti et al. [2021], and Di Traglia et al. [2024]. According to Di Traglia et al. [2024] intense Vulcanian activity (eventually accompanied by the emplacement of lava flows) between 900 AD and 1250 AD deposited the thick Palizzi sequence. This was followed by deposition of the Brecce di Commenda products (1250–1300 AD) [Rosi et al. 2018; Di Traglia et al. 2024], ascribed to a violent phreatic eruption occurring simultaneously with the Rocche Rosse eruption in Lipari [Di Traglia et al. 2024]. From circa 1400 AD to the early 18th century, volcanic activity concentrated both at La Fossa and at the eccentric La Forgia craters, generating a sequence of phreatic and Vulcanian eruptions [Malaguti et al. 2021; Di Traglia et al. 2024]. The last three centuries of activity comprise two long-lived eruption episodes in 1727–1739 (Pietre Cotte sequence) and 1888–1890 (Gran Cratere sequence) [Di Traglia et al. 2024], and some shorter or even discrete episodes, interspersed within rest periods of background hydrothermal activity lasting for decades (Table 1).

2.3 The La Fossa Fumarolic Field

Fumarolic activity today concentrates from vents and fractures on the volcano summit [Paonita et al. 2013]. This summit fumarolic field consists of two main adjacent zones: (i) a linear network of fractures and satellite vents that develop along the crater rim (rim fumaroles), including from west to east, the F0, GBC, F5AT, F7–8, F11 and F12 fumaroles; (ii) the inner fumaroles, located on the inner slope of the crater. This area consists of discrete vents or vents aligned along sealed fractures, embedded in an extended field of hydrothermal alteration, deposition and mineralization [Müller et al. 2021]. The FA fumarole, situated near the inner crater of the 1888–1890 eruption and extending toward the inner crater wall, has traditionally been the main degassing spot in the inner fumarolic field. The central-eastern section of the rim fumaroles is surrounded by a dark grey impermeable crust, and bleached surface at a distance representing areas of increased diffuse surface gas flux [Müller et al. 2021; 2024]. In addition, a small degassing area (the outer fumaroles; Figure 1E) is also located within and along the outer rims of the eccentric La Forgia craters. Degassing occurs not only through fractures and vents but also via diffuse soil degassing, affecting the areas near the rim fumaroles, both inside and outside the crater [Pailot-Bonnétat et al. 2023, and references therein]. This diffusive output [Chiodini et al. 2005; Harris et al. 2009; Inguaggiato et al. 2012; 2018; Mannini et al. 2019; Pailot-Bonnétat et al. 2023] contributes 5 to 13 MW, or circa 93% of the total volcano heat budget. The latter is thought to be sustained by convection of magmatic-hydrothermal fluids through a heat chimney composed of fractured feeding conduit rocks [Har-

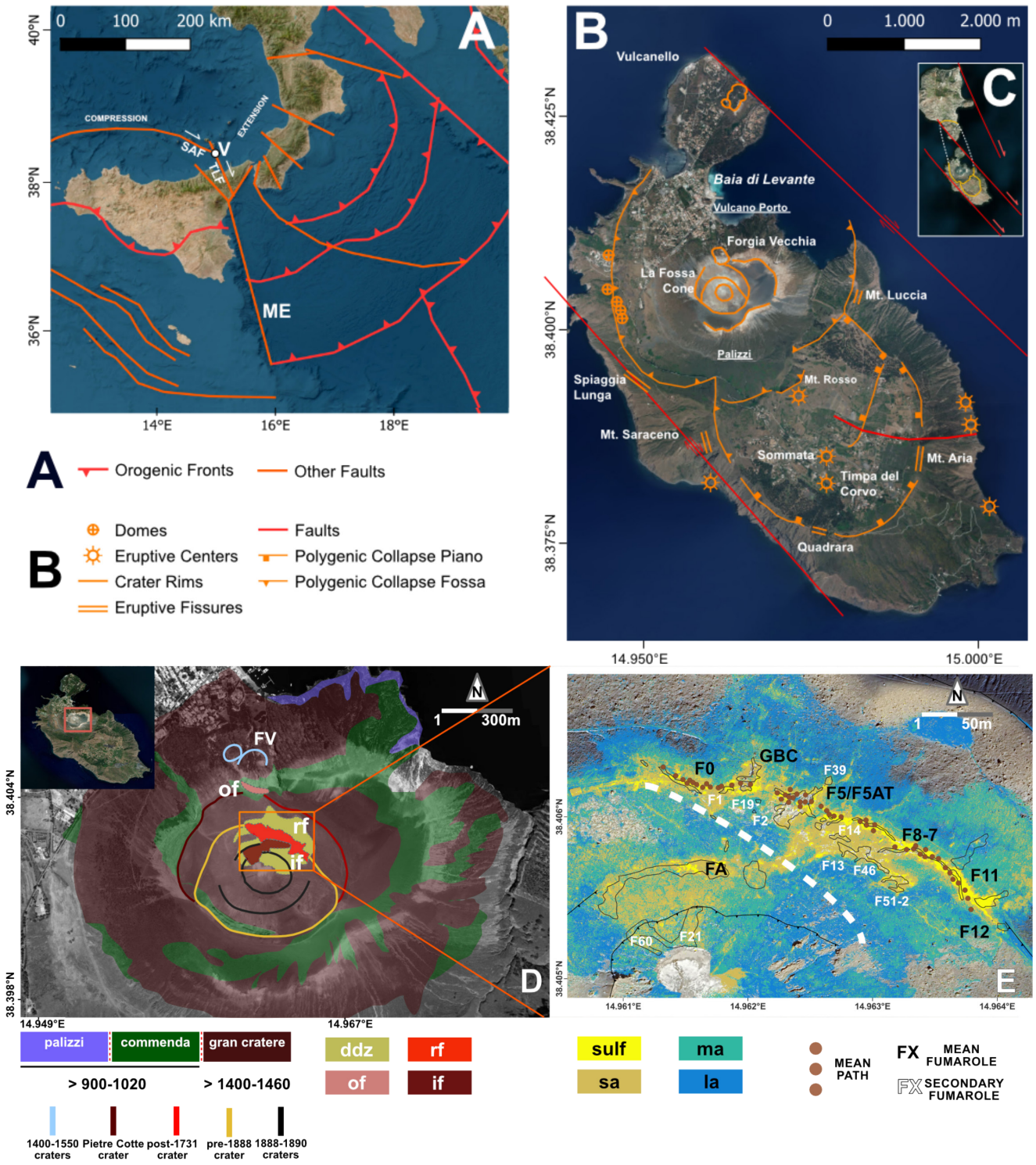

Figure 1: (Caption next page.)

ris and Maciejewski 2000; Müller et al. 2021; Pailot-Bonnétat et al. 2023], while conduction prevails in the last few meters. Such inner structure of the La Fossa cone, and especially the ascent pathways of magmatic-hydrothermal fluids, has been reconstructed and modelled using electrical resistivity tomography, self-potential, temperature, and diffuse degassing measurements [Revil et al. 2008; Barde-Cabusson et al. 2009; Revil et al. 2010]. Variations in temperature and number of fumaroles, although less influential on the overall energy balance, provide fundamental indication of the state of the system, signaling heating or cooling phases [Chiodini et al. 2005; Harris et al. 2009; Diliberto 2013; Madonia et al. 2016; Mannini et al. 2019; Pailot-Bonnétat et al. 2023; Diliberto et al. 2024].

Figure 1: (Previous page.) [A] Tectonic sketch of Sicily and nearby areas illustrating the major faults and different orogenic fronts; the strike-slip faults Sisifo–Alicudi (SAF) and Tindari-Letoianni (TLF), along with their junction at Vulcano-Lipari (V), are highlighted. SAF and the TLF forms a transfer zone that channels tectonic stresses from the compressional area west of the Aeolian Islands toward the Ionian subduction zone in the south. The interaction of SAF-TLF junction with an extensional belt to the east (Vulcano Gioia Basin-Paola Basin) produces N–S-trending structures on Lipari and Vulcano that favour the ascent of deep fluids (panels B and C). Reworked from Ruch et al. [2016] and Mantovani et al. [2023]. [B] Volcano-tectonic sketch of Vulcano Island with major eruptive centers, fissures, polygenic collapses defined by volcano-tectonic circular faults (il Piano 1-2 and La Fossa 1-2-3-4). Reworked by De Astis et al. [2013]. [C] Volcano-tectonic sketch of the islands of Lipari and Vulcano. Reworked by Holohan et al. [2008]. [D] The main units of the La Fossa cone, as inferred by Di Traglia et al. [2024]. The La Fossa cone consists of the superposition of multiple units (cones in the geomorphological sense, lithosomes in the stratigraphic sense), separated by craters of different ages that overlap to create a nested crater. Age of the craters inferred from Di Traglia et al. [2013]. The La Fossa cone summit hosts three main fumarolic zones: a marginal one on the rim of FV (outer fumaroles, of); the (rim fumaroles, rf) on the 1731–1888 crater rim; and the inner crater fumaroles (if). The rim and inner crater fumaroles are surrounded by an alteration zone in which diffuse degassing occurs (ddz). A detail of the rf and if fumaroles showing the boundary between the hotter, more magmatic (lower CO_2/SO_2 ratio) rf and the colder, more hydrothermal if. Dots indicate the crater rim traverse (results displayed in Figure 7). [E] Map of inner and rim fumaroles with nomenclature and outlines of fumaroles; in this area are presents sulfur deposits (sulf) surrounded by areas of strong (sa) to moderate (ma) to slight (la) alteration. Figure E is adapted from Müller et al. [2024].

Table 1: The last three centuries of volcanic activity at Vulcano (data from Selva et al. [2020] and Di Traglia et al. [2024]).

Type of activity	Period of activity
Long-lived eruptive periods	1727–1739 and 1888–1890
Shorter/discrete eruptive episodes	1771, 1783, 1786, 1823–1824, 1873, 1876, 1878–1879 and 1886
Quiescence and fumarolic activity periods	1740–1770, 1772–1782, 1783–1786, 1787–1832 1873–1876, 1879–1885 and 1886–1887

Magmatic gases released by the fumarolic system are thought to be source by magma stored in a complex, transcrustal plumbing system. Consensus exists for the presence of deep magma storage zone of basaltic to shoshonitic magma at 12–20 km depth b.s.l. (below sea level), overlain by an intermediate latitic magma reservoir at 3–5 km depth b.s.l., and by a shallow K-trachyte/rhyolite reservoir at 1–2 km depth b.s.l. [De Astis et al. 2013; Peccerillo 2017; Selva et al. 2020; Aiuppa et al. 2022]. Upon ascent, these magmatic fluids get admixed with steam boiled off from seawater-derived hydrothermal brines [Nuccio et al. 1999; Nuccio and Paonita 2001].

2.4 The 1987–1993 and 2021–present unrest

After the 1888–1890 eruption, La Fossa entered a state of quiescence. However, degassing activity has intensified multiple times since then, with hydrothermal unrest being recorded in 1916–1924, 1977–1980, 1987–1993, 2004–2005, and 2009 [Selva et al. 2020; De Astis et al. 2023]. A major unrest, associated with macroscopic changes in the fumarolic field, was observed between 1987 and 1993 [Barberi et al. 1991]. At that time, new fractures (F0, GBC, F11, F12, satellite fractures) formed and existing fractures (FA, F5AT, F7–8) expanded and reorganized, in parallel with substantial changes in fumarole composition and flux, and seismicity [Italiano et al. 1998; Alparone et al. 2010; Harris et al. 2012; Diliberto 2017]. Fumarole temperature increased from 435 °C in 1988 to 692 °C in 1992, before dropping again to 428 °C in 1999. During this period, the fumarolic field expanded towards the bottom of the crater as the FA area grew [Harris and Maciejewski 2000; Diliberto 2017]. Fumarolic gas composition also varied substantially, indicating an increased contribution of magmatic volatiles and (potentially) a change in hydrothermal fluid conditions from biphasic to dry gas conditions [Chiodini et al. 1993; Chiodini et al. 1995; Nuccio et al. 1999; Paonita et al. 2002].

The most recent hydrothermal unrest at Vulcano started in September 2021 [Federico et al. 2023], when an abrupt increase in thermal [Coppola et al. 2022; Inguaggiato et al. 2022; Pailot-Bonnétat et al. 2023; Campus et al. 2024; Diliberto et al. 2024] and gas [Aiuppa et al. 2022; Di Martino et al. 2022; Inguaggiato et al. 2022; Federico et al. 2023; Inguaggiato et al. 2023; Giuffrida et al. 2025] output was observed. According to Pailot-Bonnétat et al. [2023] and Diliberto et al. [2024], the main hydrothermal unrest may have been preceded by a sluggish phase of soil/fumarole increase starting as early as February 2021. Inguaggiato et al. [2022] also found a precursory phase of soil CO_2 emission increase beginning in early 2021. During the main (post-September 2021) phase of the unrest, fumarole composition manifestly became more CO_2- and S-rich (more magmatic), as also indicated by He isotope compositions in the fumaroles [Federico et al. 2023]. Among the lowest ever measured CO_2/S_T ratios (10–15) at Vulcano were observed during fall 2021, confirming a more magmatic signature and a reduced hydrothermal processing [Aiuppa et al. 2022]. Later in winter–spring 2022, the unrest manifested also at the base of La Fossa and in the nearby Baia di Levante hydrothermal area, where a general increase in gas output resulted into significant environmental and health impact when CO_2 and H_2S concentrations in soil and air rose to potentially hazardous lev-

els for the population [Di Martino et al. 2022; Inguaggiato et al. 2022; 2023]. In some wells in the Vulcano Porto village, water temperatures close to 70 °C were recorded [Inguaggiato et al. 2023] and, between September 2021 and May 2022, the CO_2 flux increased 32-fold in the crater, and 15-fold in the Baia di Levante area compared to local background values. The anomaly delay between the crater and peripheral areas has been interpreted as due to the interaction with local shallow hydrothermal aquifers, which may have buffered the ascent of fluids until saturation was reached, at which point gas would have been able to migrate toward the surface [Di Martino et al. 2022; Inguaggiato et al. 2022]. One notable effect was the appearance of a milky-white seawater coloration in the Baia di Levante bay offshore [Coppola et al. 2022], which was caused by the presence of suspended fine mineral particles (sulfides and sulfates) that precipitated in the water column in response to increased hydrothermal fluid inflow. Geophysical data indicate that the La Fossa unrest was associated with mild ground uplift [Di Traglia et al. 2023; Federico et al. 2023] and in shallow VLP (Very Long Period) seismicity [Federico et al. 2023]. These were interpreted as due to pressurization of the shallow (<1 km) hydrothermal system by rising magmatic fluids. Di Traglia et al. [2023], using GNSS and InSAR time-series data, modelled the inflation source as a dipping prolate spheroid model located at a depth of 600 m, pressurized by magmatic fluids. Fluid migration along N–S-trending fractures may have favoured extension of the area affected by the unrest in the following months. Volcano-tectonic (VT) seismicity was moderate in fall 2021 [Federico et al. 2023].

Pailot-Bonnétat et al. [2023] interpreted the unrest as caused by the following sequence of events. A mild increase in magmatic fluid input into the shallow hydrothermal system may have started as early as January–June 2021, as evidenced by soil temperature records. The increase in magmatic fluids led to gradual formation of a gas chimney and to a slow rise in heat flux, which was initially confined to within the partially sealed fracture network that had developed beneath the Fossa fumarolic field during and after the 1988–1996 unrest. However, starting in spring 2021, the emission area gradually expanded toward the peripheral zones of the fumarolic field and, at the beginning of September 2021, the impermeable seal surrounding the chimney failed due to fracturing, triggering VLP swarms and causing a sudden and significant expansion of the thermal and gas output. In addition to Di Traglia et al. [2023], Stumpp et al. [2024] also imaged a sub-vertical conduit with very low S-wave velocities (0.8 km/s), extending to a depth of at least 2.5 km, which would have acted as the transport feeding conduit for the ascent and pressurization of magmatic gases during the unrest. The unrest gradually vanished in 2023-to-present, as evidenced by decreasing gas fluxes [Inguaggiato et al. 2023; Giuffrida et al. 2025] and composition/temperature records [*INGV monitoring reports*].

3 Methodology

The results we report on this study are obtained from periodic field surveys using a portable Multi-GAS [Aiuppa et al. 2005; Aiuppa et al. 2007], complemented with thermal infrared results obtained from drone surveys. The Multi-GAS unit used has the same configuration as that employed by Aiuppa et al. [2022], and includes a non-dispersive infrared (NDIR) NG Gascard spectrometer (calibration range, 0–10,000 ppm) from Edinburgh Sensors for CO_2, and three CiTiceL electrochemical sensors for SO_2 (model T3STF), H_2S (model T3H) and H2 (model T3HYT) (all having 0–200 ppm calibration range). All sensors were calibrated in the laboratory prior to and after field work using certified standard gases, finding a typical uncertainty/precision of ~±5% at the concentration levels encountered at Vulcano. The system also includes a KVM3/5 Galltec-Mela sensor for measuring temperature and relative humidity and to indirectly estimate H_2O concentrations in the plume using the Arden-Buck equation [Buck 1981], which calculates the saturation vapor pressure of water as a function of temperature. A Campbell CR6 datalogger acquires signals from the various sensors at 1 Hz rate and stores them on an SD card (data are also Wi-Fi transferred and visualized in real-time in external palm). Equipment is housed in a water-proof case.

In the field, the portable Multi-GAS unit (<3 kg) is carried by an operator across the field, continuously acquiring data at 1 Hz, and with position recorded by a GPS synchronized at the start of the instrumentation. Acquired gas concentration data is displayed in real-time on an external palm-sized device. The fumarolic field is then traversed by walk with the held-hand Multi-GAS, while keeping the instrument's inlet exposed to the gases at 50 cm distance from the vent to avoid sensor saturation. Each fumarolic vent is monitored for a few minutes, and the different fumaroles are analysed sequentially to cover the entire field in about an hour. The range and diversity of gas concentrations over the fumarolic field is then determined and mapped (Figures 2–3).

The gas concentration time-series acquired within each campaign are processed using a processing routine [Aiuppa et al. 2021; 2022], written in R*. This routine automatically scans the gas concentrations time series, searching for periods of high temporal coherence ($R^2 \geq 0.7$) between couples of gas species in 60 s long moving windows. Specifically, within each of such sequentially scanned time windows, the routine calculates a ratio (for example, the CO_2/SO_2 ratio) if two criteria are met: (i) the Pearson correlation coefficient is ≥0.7 and (ii) the SO_2 concentration threshold of 20 ppm is reached [Aiuppa et al. 2022]. The obtained georeferenced ratios are finally illustrated in the form of either contour (Figure 4) or dotted (Figure 5) maps.

Eleven field campaigns were realized between 2021 and 2024, and the results are illustrated in Supplementary Material 1. To illustrate the temporal evolution of the fumarolic field, four illustrative maps are shown in Figure 4 where, for comparison, we also present the (unpublished) results of two campaigns conducted in April 2014 and June 2018 that correspond to periods of background (reduced) degassing activity (as indicated by *INGV monitoring reports*), and SO_2 flux results; Giuffrida et al. [2025]). Because of accessibility and time constraints, the area covered by observations varies from one survey to another (Figure 4 and Supplementary Material 1). However, all surveys cover the crater rim area where the

*https://www.r-project.org/

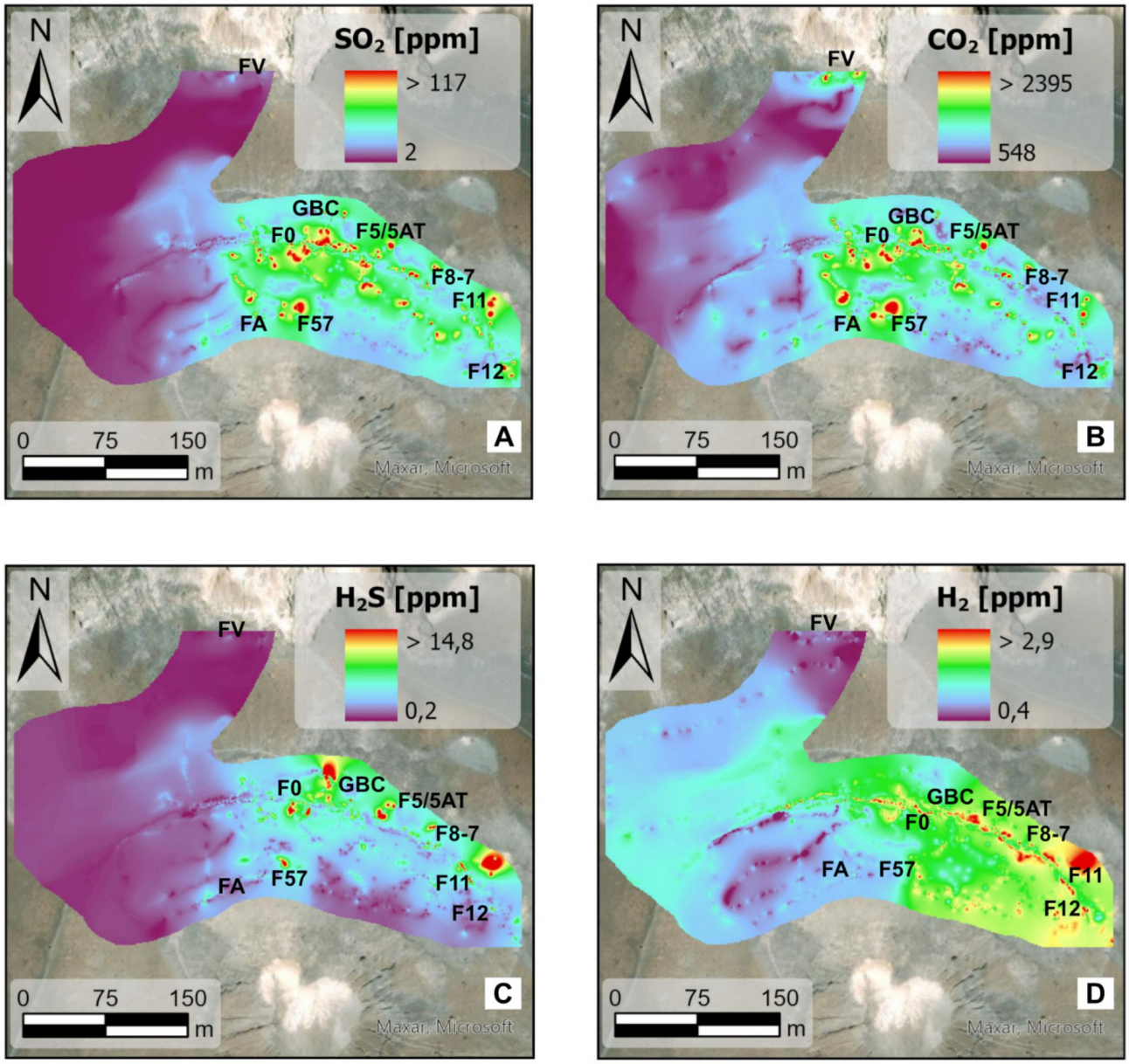

Figure 2: SO_2, CO_2, H_2S and H_2 concentration maps (June 2024 campaign). The most actively degassing fumaroles are identified as peak gas concentration spots.

hottest and most actively degassing fumaroles have been active in the last decade(s), e.g. since when fumarolic activity in the inner FA fumarole declined after the 1987–1993 unrest.

As a complement to Multi-GAS records, thermal infrared data were acquired using a FLIR Tau 2 radiometric thermal infrared camera system mounted on a DJI Phantom 4 Pro. The FLIR Tau 2 is a fully radiometric sensor system with a sensor resolution of 640 × 512 pixels. It measures in the thermal infrared spectral range between 7.5 and 13 µm. The data is recorded by a TEAX Thermal Capture 2 data logger at 8 Hz and geotagged using an external GPS antenna. Infrared data acquisition is performed by flying in loops at a constant altitude over the target area, ensuring a minimum overlap of 65% for each image. This is necessary for subsequent photogrammetric processing. The data were then inspected and quality checked in ThermoViewer (version 3.0.0), and images of poor quality or out of focus were excluded. Quality check also included selection of images taken at constant flight attitude. The selected images were exported in 16-bit greyscale tiff format and processed in Agisoft Metashape to produce a thermal mosaic covering the central crater region of La Fossa cone.

We also report on a SO_2 flux time-series from La Fossa crater (Figure 6) obtained by a fixed UV Camera system located at Orsa Maggiore Hotel, ~1.49 km NW from the summit. Functionalities of this fully autonomous UV camera system are described in Aiuppa et al. [2022]. In brief, the unit assembles two JAI CM-140GE-UV cameras sensible to UVradiation, fit-

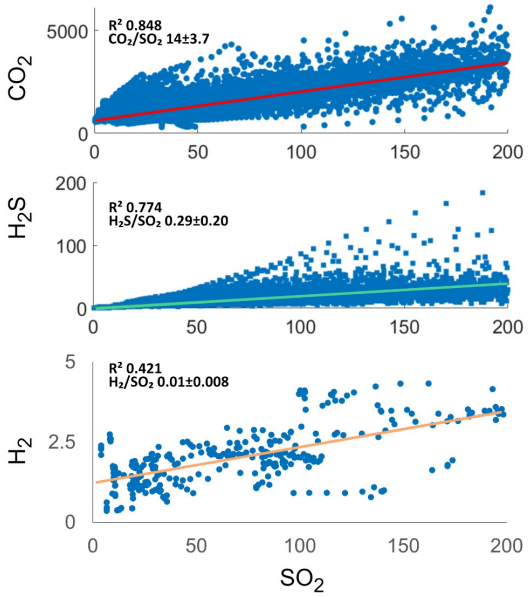

Figure 3: Scatter plot of SO_2 vs. [A] CO_2, [B] H_2S and [C] H_2 concentrations.

ted with two distinct band-pass optical filters (both of 10 nm Full Width at Half Maximum) with central wavelengths of 310 (SO_2 absorption) and 330 nm (no SO_2 absorption) [Delle Donne et al. 2016; 2019; Lo Bue Trisciuzzi et al. 2024]. Images are simultaneously acquired by the two cameras at 0.5 Hz. During post-processing, sets of co-acquired images are combined into absorbance images that are later converted into calibrated slant column amount (SCA) images. From this, integrated column amounts (ICA) time-series are obtained by integration along a cross-section perpendicular to plume transport. The SO_2 flux time is finally derived by multiplying ICA by plume speed, as derived by tracking the motion of plume gas fronts in image sequences, using an optical flow algorithm [Delle Donne et al. 2016; 2019; Lo Bue Trisciuzzi et al. 2024]. Uncertainty is evaluated at ~±30%, and is mainly determined by radiative transfer issues (e.g. light dilution effects and in-plume scattering effects; Kern et al. [2010]). Results shown in Figure 6 are daily averages calculated over temporal windows with optimal viewing conditions (clear sky, high plume visibility, uncondensed plume).

4 Results

4.1 Chemical structure of the fumarolic field

In a dedicated campaign in June 2024, the entire La Fossa fumarolic field was covered by a series of Multi-GAS walking traverses released during four measurement days (June 19th, 24th, 25th and 26th). This detailed survey allows the chemical structure of the fumarolic field to be fully reconstructed and visualized. Results are shown in the gas concentration maps of Figure 2, which are based on the interpolation of 16,779

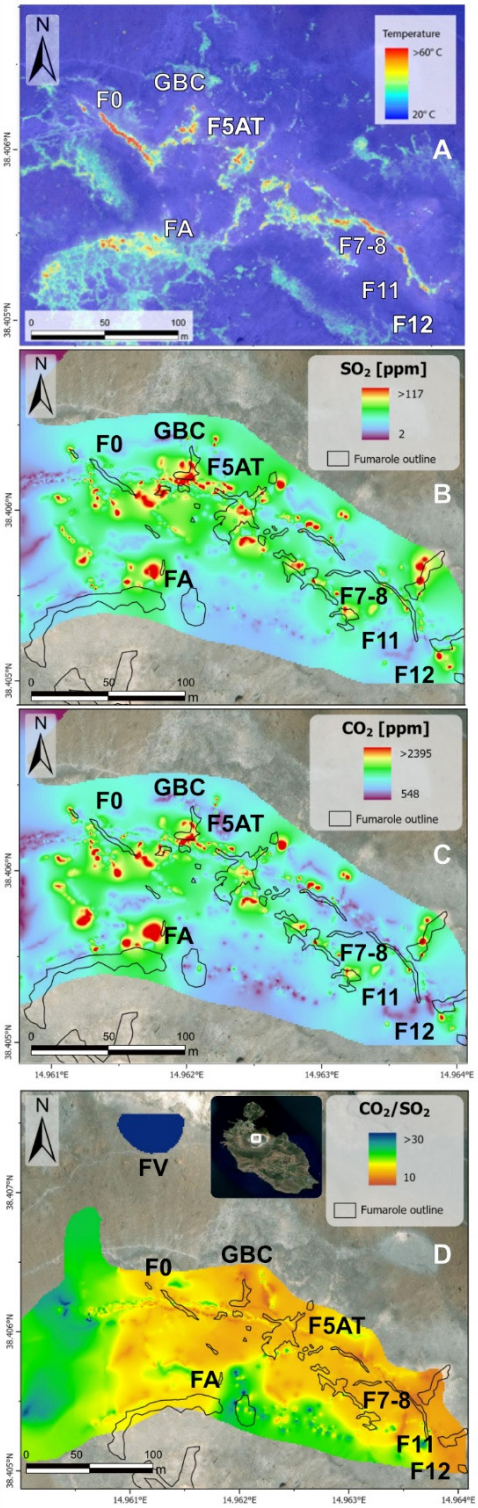

Figure 4: [A] Drone thermography of the fumarolic field, taken on October 20th 2021. The locations of the main degassing fissures and vents, as indicated by peak apparent temperatures, broadly correspond to the peak SO_2 [B] and CO_2 [C] concentration spots, as revealed by the Multi-GAS measurements. The CO_2/SO_2 ratio map [D] shows the contrast between the rim fumaroles (lower ratios) and the peripheries of the fumarolic field (higher ratios). FV identifies the Forgia Vecchia fumaroles.

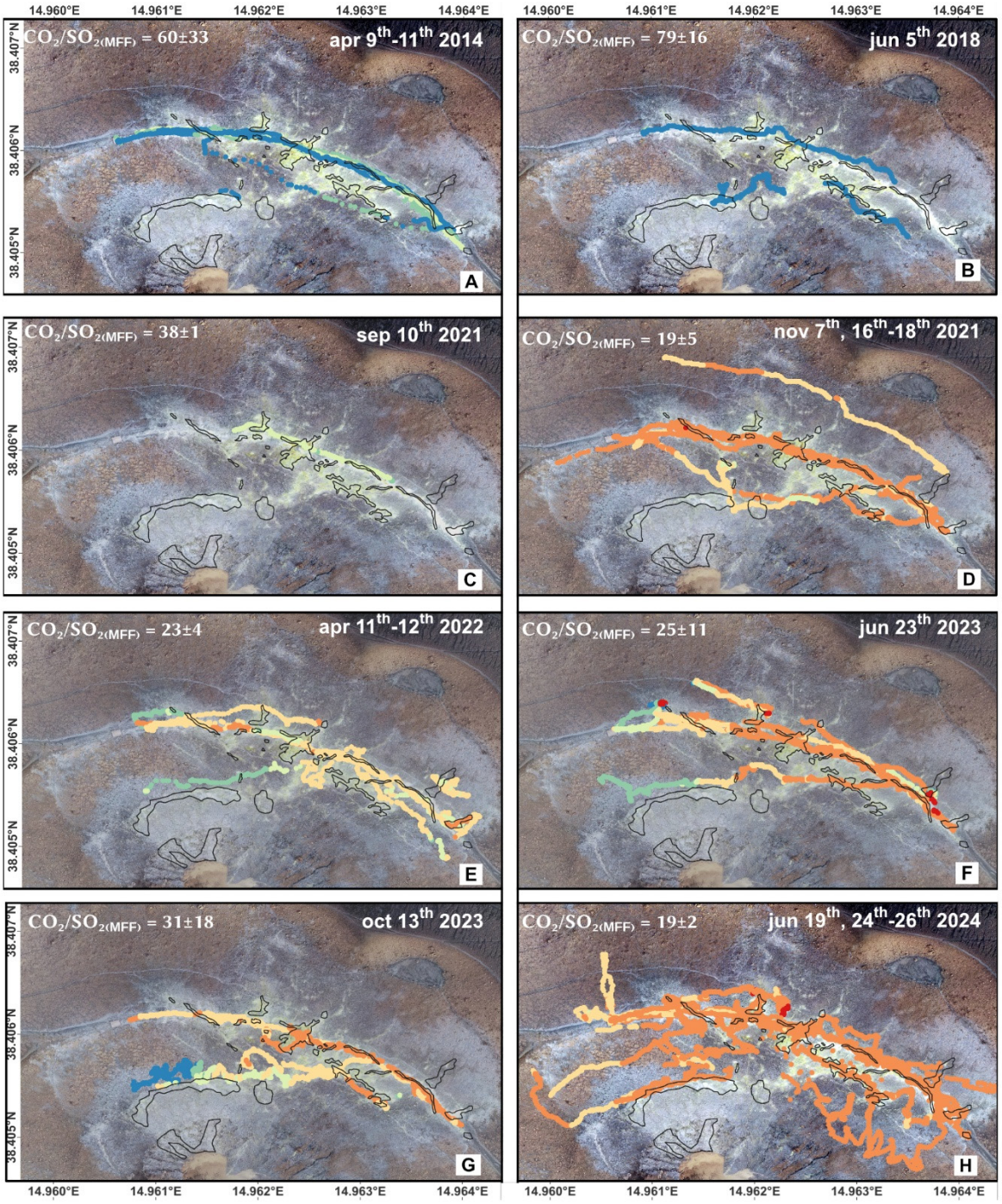

Figure 5: Selected dotted maps of the CO_2/SO_2 ratio in the La Fossa fumarolic field, obtained in eight distinct campaigns between September 2021 and June 2024. For reference, the upper two panels illustrate results for the April 2014 and June 2018 surveys, here taken as representative of phases of background hydrothermal activity (e.g. with limited transport of sulfur-rich magmatic gases). The eight maps shown are extracted from the whole dataset shown in Supplementary Material 1. The CO_2/SO_2 values in the maps are plotted using a color scale in which red tones are representative of magmatic compositions ($CO_2/SO_2 < 10$; Aiuppa et al. [2022]) while deep blue tones correspond to hydrothermal gas compositions ($CO_2/SO_2 \gg 30$). Intermediate color tones indicate intermediate CO_2/SO_2 ratio compositions, as typical of mixed magmatic-hydrothermal compositions. All maps realized in QGIS (https://qgis.org/).

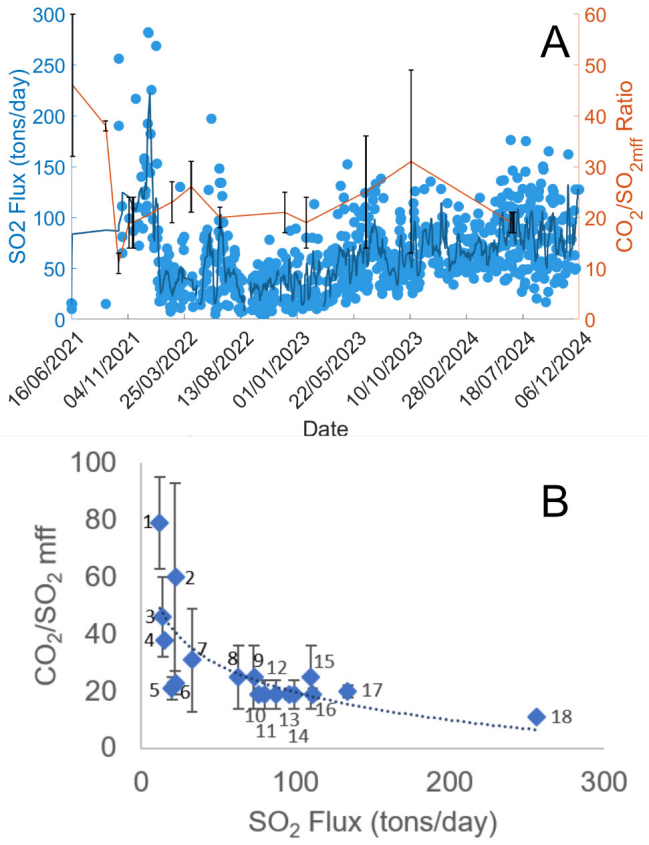

Figure 6: [A] Temporal record of the SO_2 flux (in tons/day) and of the $CO_2/SO_{2(MFF)}$ ratio (from the maps of Figure 5 and Supplementary Material 1). The blue line is a moving average of the SO_2 flux. A scatter plot comparing the two parameters is shown in [B]. 1: June 5th 2018; 2: April 12th 2014; 3: June 19th 2021; 4: September 10th 2021; 5: December 1st 2022; 6: February 23rd 2022; 7: October 13th 2023; 8: June 22nd 2023; 9: June 23rd 2023; 10: June 24th 2024; 11: January 24th 2023; 12: November 18th 2021; 13: June 25th 2024; 14: November 7th 2021; 15: June 21st 2023; 16: June 19th 2024; 17: June 22nd 2022; 18: October 12th 2021.

individual Multi-GAS measurements of each of the species determined (SO_2, CO_2, H_2S and H_2). Data interpolation is realized using the inverse distance weighting (IDW) interpolation method, which assumes that the relative weight of each measurement on its surroundings diminishes with distance (d) according to a power law of the type d^{-p}, where $p = 2$ in our case. To limit spatial interpolation to areas reasonably close to the measurement path, a barrier polygon function is used. We yet caution that since IDW assumes isotropic spatial influence, while gas outflow is controlled by the anisotropic distribution of fractures, topographic lineaments and wind pattern, physical processes such as gas channeling (by fractures) and atmospheric dispersion are not taken into account, which means the maps do not capture geological realities in full. Still, our maps clearly locate the positions of the most actively degassing fumaroles as visible spots of high gas concentrations (Figure 2).

We find the main degassing areas in the eastern portion of the investigated area, along the post-1731, 1888–1890 crater rim (see Figure 1D) and in the inner crater area connecting the F0 and FA fumarolic areas. The peak concentrations observed are respectively 193 ppmv (SO_2), 4521 ppmv (CO_2), 117 ppmv (H_2S) and 4.1 ppmv (H_2). Hydrogen and (to a lesser extent) H_2S show no evident peaks in the FA area and hence are mostly degassed by the rim fumaroles. In contrast, lower, closer-to-background gas concentrations are observed in the western-most segment of the surveyed area, where strongly altered, mineralized rocks with minimal (if any) fumarolic activity prevail. A secondary CO_2 concentration peak is observed in the northern-most part of the surveyed area, in correspondence with the southern area of the Forgia Vecchia explosion vents (FV in Figure 1D).

The scatter plots of Figure 3 highlight the correlation between the four gases species but also show large scatter indicative of chemical diversity in the fumarolic field. The CO_2/SO_2 ratios (Figure 3A) in June 2024 range between 7 and 29 (the slope of the best fit regression line is 14.1 ± 3.7). SO_2 prevails over H_2S over the entire fumarolic system (the average H_2S/SO_2 ratio for the fumarolic system is 0.29 ± 0.20; Figure 3B) except in the proximity of the Forgia Vecchia area. The average H_2/SO_2 ratio is $(9 \pm 6) \times 10^{-3}$ (Figure 3C).

Figure 4 illustrates a zoomed view of the apparent temperature of the fumarolic field (Figure 4A), in comparison to the main SO_2 and CO_2 concentration peaks are identified in a narrow NW–SE-oriented area stretching between the F0, GBC and F5/F5AT fumaroles. High SO_2 and CO_2 concentrations are also observed in the atmospheric plumes of F11, F12 and FA fumaroles (Figure 4B and 4C). Overall, there is good correspondence between the most actively degassing areas (the gas concentration peaks) and the area of most intense thermal anomaly, as identified by the drone-based thermal map of Figure 4A. The contour map of Figure 4D shows a broad range of relativity homogeneous and prevailing low (mean, 19 ± 2) CO_2/SO_2 ratios over the entire crater rim area. In contrast, higher CO_2/SO_2 ratios (range, 20–26), indicative of more hydrothermally processed compositions, are observed in at westernmost margin of the fumarolic field, and in the intra-crater sector comprised between the FA, F13 and F12 fumaroles.

4.2 Temporal evolution of the fumarolic field

The maps of Figure 5 offer a graphical representation of the evolution of the fumarolic field during the study period. In the maps, color tones are adapted to convey information on the temporal alternation between phase of high (green to blue tones) and low (orange to red) CO_2/SO_2 ratios. In each of the maps, the spatial variations of color tones provide clues on the spatial variations of the CO_2/SO_2 ratio over the fumarolic field, and hence on its spatial homogeneity/heterogeneity. For each map, the average ratio (±1 standard deviation), calculated as the arithmetic mean of all the ratios across the entire field (referred as $CO_2/SO_{2(MFF)}$), is also reported.

Figure 5A and 5B are examples of CO_2/SO_2 ratio maps taken in periods of reduced (background) hydrothermal activity at La Fossa, e.g. April 2014 and June 2018. In both

periods, the fumarolic field exhibits uniform and high (>50) CO_2/SO_2 ratios, both in crater rim and inner crater fumaroles (same as for the May 2017 survey; see Supplementary Material 1C). This chemical homogeneity of the fumarolic field is graphically illustrated by the dominance of blues color tones. In quantitative terms, the mean fumarolic field (MFF) ratio is ≈80.

In contrast, Figure 5D is a map of the CO_2/SO_2 ratio taken in November 2021, near the acme of the La Fossa 2021 unrest [Federico et al. 2023]. Here, low ($10 < CO_2/SO_2 < 20$) to locally very low ($CO_2/SO_2 < 10$) ratios are observed over the entire crater rim area. In contrast, the inner and outer crater fumaroles are associated with intermediate (20 to 30) CO_2/SO_2 ratios. The $CO_2/SO_{2(MFF)}$ in November 2021 is ≈19. Importantly, results for the June 2021 (Supplementary Material 1F) and September 2021 (Figure 5C) surveys, made only a few months/days prior to the unrest onset (nominally fixed in the second half of September; Coppola et al. [2022], Di Traglia et al. [2023], and Federico et al. [2023]), still exhibit the prevalence of high-very high (June: $CO_2/SO_{2(MFF)} \approx 46$) to intermediate (September: $CO_2/SO_{2(MFF)} \approx 38$) CO_2/SO_2 ratios, confirming the abrupt onset of the unrest.

Surveys taken after November 2021 (Figure 5E–5H and Supplementary Material 3 and Supplementary Material 4) demonstrate persistence of the unrest, yet at alternating levels. Broadly speaking, the dominance of orange color tones in the February 2022 to June 2024 maps supports the persistence of intermediate (20 to 30) CO_2/SO_2 ratio compositions in the fumarolic field. However, our results also reveal the alternation of periods of declining unrest, e.g. from November 2021 to February 2022 and in April 2022 during which a progression toward higher CO_2/SO_2 ratios are observed, with periods of accelerating unrest, when CO_2/SO_2 decrease again (e.g. June to December 2022 and June 2024). We also find that while the crater rim fumaroles exhibit relatively invariant CO_2/SO_2 ratios throughout February 2022 to June 2024 (except perhaps in April 2022), the inner crater fumaroles show larger temporal variability, especially those in the western sector of the fumarolic field (Supplementary Material 3 and Supplementary Material 4). An especially large compositional diversity in the fumarolic field, with a west to east progression from high/very high ratios to low ratios, is observed in the June 2023 and October 2023 maps (Supplementary Material 3 and Supplementary Material 4).

Figure 6 explores the relationship between the $CO_2/SO_{2(MFF)}$ and the daily-averaged SO_2 flux. Figure 6A shows that the SO_2 flux increased from 14 ± 3 tons/day in June–early September 2021 to 135 ± 60 tons/day in October–November 2021. The SO_2 flux then decreased to <50 tons/day in early 2022, paralleled by a $CO_2/SO_{2(MFF)}$ increase to ~23 in April 2022 (Supplementary Material 1). A new pulse of SO_2 flux increase (to >100 tons/day) was then observed in fall 2021–summer 2022, contemporaneous with onset of the degassing unrest at the peripheral Baia di Levante hydrothermal site [Coppola et al. 2022; Federico et al. 2023; Inguaggiato et al. 2023]. After a relatively low SO_2 flux phase in late 2022 to early 2023, the SO_2 flux progressively and moderately increased from May 2023, and stabilized to levels of 50–100 tons/day from the onward. The $CO_2/SO_{2(MFF)}$ fluctuated at intermediate levels of 20 to 30 in the same temporal interval (Figure 6A). Overall, the SO_2 flux vs. $CO_2/SO_{2(MFF)}$ dependency (Figure 6B) identifies a background state for the fumarolic field associated with low (<30 tons/day) SO_2 fluxes and high (hydrothermal) $CO_2/SO_{2(MFF)}$ ratios (>50) that is clearly distinct from a "degassing unrest" population, with high (>50 tons/day) SO_2 fluxes and low (<30) $CO_2/SO_{2(MFF)}$ ratios. The most-magmatic compositional pole (SO_2 fluxes of >250 tons/day and $CO_2/SO_{2(MFF)}$ ratios of circa 10) is exemplified by the October 2021 composition.

4.3 Evolution of the crater rim fumarolic zone

While the fumarolic field was irregularly covered in the different field campaigns, the crater rim area was more systematically investigated, allowing more careful analysis. Therefore we present the results (Figure 7) for compositional variations along a 370 m long "rim crater path", traversing 54 individual measurement points (shown in Figure 1E) across the crater-rim in a roughly west-to-east direction. The path starts at F0 and crosses GBC fumaroles, the central part of F5AT, F8 fumaroles and ends at the fumaroles F11. For simplicity and for improving readability of the figure, results of surveys taken in the same year are averaged except for 2021 (to more finely resolve gas composition variation at the unrest onset), and a smoothing (3 points mobile average) is applied.

Results (Figure 7) demonstrate relatively uniform (spatially invariant) CO_2/SO_2 ratios along the crater rim during background activity (see 2014 and 2018 lines). In June 2021, ~3 months before initiation of the unrest, the crater rim fumaroles exhibited wider compositional diversity, with a progression toward intermediate ratios in the western (F0 area; <0.05 km distance) and central (F5–F7 area; 0.15–0.25 km distance range) segments of the transect (see also Figure 8). By early September 2021, just a few days/weeks prior to the unrest onset, the crater rim fumaroles had homogenized to intermediate ratios of circa ~38 (Figure 7; see also Figure 5). From November 2021 to June 2024, we observe a remarkable chemical homogeneity of the crater rim fumarolic field at lower (more magmatic) ratios of 15 to 30 (Figure 7), with important implications discussed below.

5 Discussion

Chemically profiling a fumarolic field with a real-time sensing Multi-GAS unit provides intrinsically less precise results than reachable with traditional direct sampling, and especially poses severe limitations to the number of chemicals that can be analysed. During unrest, however, expedited Multi-GAS surveys can be beneficial in reducing exposure of operators to toxic gases, and can help reconstructing the chemical diversity of the fumarolic field by rapidly analysing a far larger number of fumaroles than accessible with direct sampling.

In the extremely well monitored 2021–present La Fossa unrest [Federico et al. 2023], Multi-GAS surveys can complement available gas information by imaging (Figures 2, 4–8) the spatio-temporal evolution of the fumarolic field, hence contributing to interpreting dynamics and evolution of the unrest.

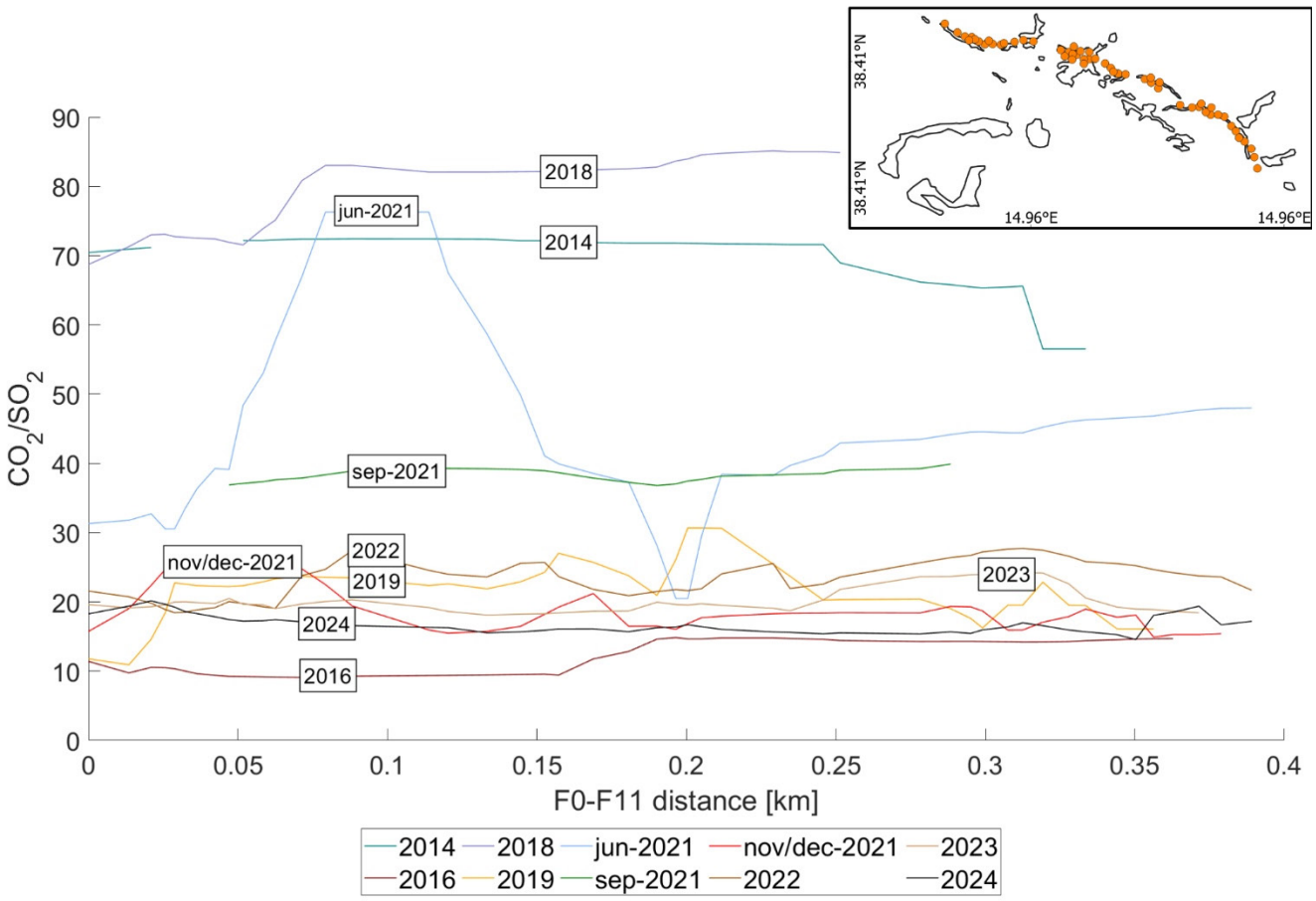

Figure 7: Moving-averaged CO_2/SO_2 ratios along a crater rim transects stretching from F0 to F11. Except for 2021, data obtained in different campaigns in the same year are averaged to obtain averaged yearly trend. 1: June 5th 2018; 2: April 12th 2014; 3: June 19th 2021; 4: September 10th 2021; 5: December 1st 2022; 6: February 23rd 2022; 7: October 13th 2023; 8: June 22nd 2023; 9: June 23rd 2023; 10: June 24th 2024; 11: January 24th 2023; 12: November 18th 2021; 13: June 25th 2024; 14: November 7th 2021; 15: June 21st 2023; 16: June 19th 2024; 17: June 22nd 2022; 18: October 12th 2021.

Our results show that, within the context of the large spatio-temporal variability of the fumarolic field (Figures 2, 4–5), the crater rim fumaroles have maintained a relatively uniform (space- and time-invariant) CO_2/SO_2 ratio signature throughout 2021 to 2024 (Figures 5, 7–8). This contrasts with the southwestern portion of the fumarolic field that has experienced instead wider spatio-temporal fluctuations in composition, alternating (in both space and time) high and low CO_2/SO_2 ratio compositions (Figure 5 and Supplementary Material 1 and Supplementary Material 4). These two distinct regions are broadly separated by a NW–SE-trending boundary zone (Figure 1E), to the north-east of which more magmatic, relatively uniform CO_2/SO_2 ratios (in the 19 to 31 range) have been observed. Our results thus help confining the boundaries of the most actively degassing zone at La Fossa (Figure 3), and point to the crater rim sector as the surface expression of the magmatic gas transport conduit (the heat chimney of Pailot-Bonnétat et al. [2023]) feeding the 2021–2024 unrest. The crater rim fumarolic area corresponds to the norther edge of the cr6 crater identified by Di Traglia et al. [2013], interpreted as the outer rim of the crater that fed the post-1739 open-vent activity of La Fossa [Selva et al. 2020], including its last eruption in 1888–1890 (Figure 1D). This geological discontinuity may thus have served as a preferential gas ascent pathway for deeply rising magmatic volatiles [Federico et al. 2023], consistent with the peak fumarolic temperatures recorded there [Diliberto et al. 2024]. The 2021–present unrest hence differs from the 1988–1993 unrest, during which the peak temperatures and most magmatic gas compositions were observed in the inner crater fumarolic zone, especially in the FA fumarole area [Selva et al. 2020, and references therein]. In contrast, during 2021–2024, the space-time compositional variability observed in the FA region, and more broadly on the south-western portion of the fumarolic field (Supplementary Material 1), may be interpreted to reflect the alternation of phases of expansion (e.g. see June 2024 map) and contraction (e.g. see October 2023 map) of the gas/heat feeding conduit, in response to changes in magmatic gas supply from below,

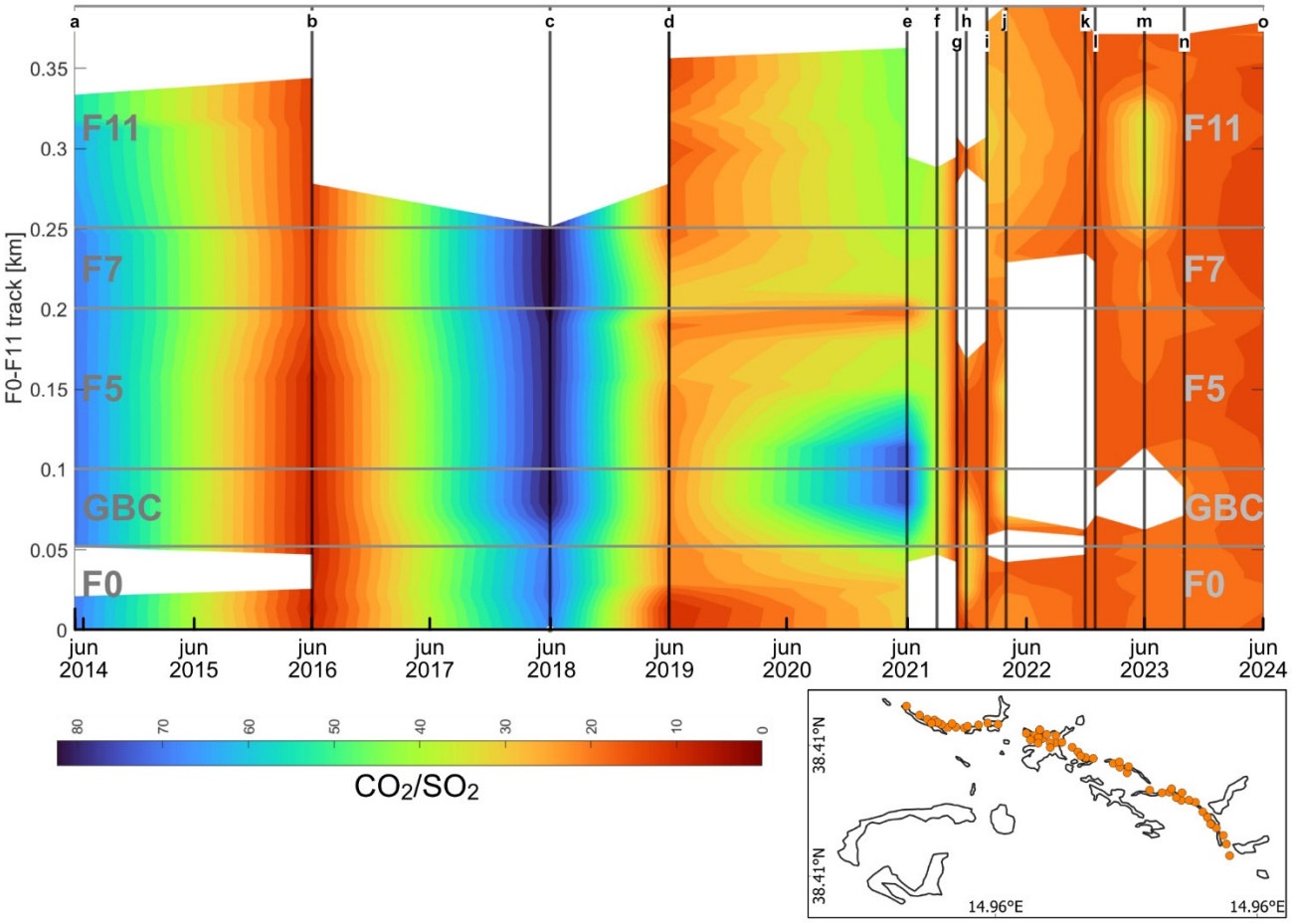

Figure 8: Mesh diagram showing the spatio-temporal evolution of the CO_2/SO_2 ratio across the crater rim fumaroles during 2014 to 2024. Time is the x-axis, distance along the F0–F11 transect on the y-scale. Color tones are proportional to the CO_2/SO_2 ratio (see legend). A remarkable compositional homogeneity of the fumarolic field is observed since the onset of the unrest in fall 2021. Letters identify the different campaigns.

and/or permeability changes in the shallow hydrothermal system [Pailot-Bonnétat et al. 2023]. As previously noted [Pailot-Bonnétat et al. 2023], the very dynamic (spatially and temporally changing) nature of the south-western margin of the fumarolic field makes it very useful target to deciphering evolution of the unrest. A compositional shift of the south-western fumaroles, from hydrothermal to magmatic, and hence a tendency toward a general compositional homogenization of the entire fumarolic field, should be viewed as potential signs of heightened future unrest at Vulcano.

Our results also contribute to interpreting the temporal evolution of the unrest. At La Fossa cone, there is a well-documented record of periodic increases in degassing activity since the late 1970s [Selva et al. 2020, and references therein]. Some of these degassing pulses have manifested in evident, macroscopic changes such as the emission of large plumes from the volcano summit, increases in toxic gases in soil and air at the volcano periphery, and/or changes in temperature, acidity and salinity of water bodies onshore and offshore [Barberi et al. 1991; Federico et al. 2023]; while some others have produced more subtle changes that could only be captured thanks to careful monitoring [Paonita et al. 2013; Inguaggiato et al. 2018]. One common aspect of these events has been their abrupt initiation, a fact that has led to models [Paonita et al. 2013] explaining unrest as caused by sudden outburst of magmatic gases previously accumulated (during quiescence) at some structural/permeability discontinuity in the shallow hydrothermal system. The implication of these models would be that unrest is essentially hydrothermal in nature, and that hence there is no upward migrating magma involved.

The more recent unrest of La Fossa also started in mid-September 2021 [Coppola et al. 2022; Di Martino et al. 2022; Inguaggiato et al. 2022; Di Traglia et al. 2023; Federico et al. 2023; Inguaggiato et al. 2023; Pailot-Bonnétat et al. 2023; Campus et al. 2024; Diliberto et al. 2024; Müller et al. 2024; Giuffrida et al. 2025], and reached its climax in October–November 2021, when a peak in degassing, seismo-volcanic activity and fumarole temperatures was reached. The lowest (<10), most

magmatic CO_2/SO_2 ratios in our dataset [Aiuppa et al. 2022] were consistently observed in this phase, associated with the largest SO_2 fluxes (Figure 6A). From late 2021 onward, degassing and seismicity at the summit slowly but progressively declined, accompanied by a progressive expansion and shift of the degassing unrest towards more peripheral areas (the Vulcano Porto plain and Baia di Levante area) in early/mid 2022 [Coppola et al. 2022; Federico et al. 2023; Inguaggiato et al. 2023]. Our results track well this declining unrest at La Fossa summit, as indicated by $CO_2/SO_{2(MFF)}$ ratios increasing again to intermediate values of 19 to 31 (Supplementary Material 1 and Supplementary Material 4) and SO_2 fluxes decreasing to <100 tons/day (expect for a phase of SO_2 flux increase in fall 2021–summer 2022 concomitant with onset of the degassing unrest at the peripheral Baia di Levante). Therefore, following a steep activity increase and peak in late 2021, a three-year long coda was observed.

In this context of vanishing unrest, we yet notice that the CO_2/SO_2 ratio levels observed at the crater rim in 2021–2024 (Figure 6–8) are still well below those observed during phases of reduced (background) hydrothermal activity at La Fossa (see for example the April 2014, May 2027 and Jun 2018 maps of Supplementary Material 1 and Supplementary Material 4 and Figure 6B), during which gases with CO_2/SO_2 ratios ≫30 (Figure 6B), and eventually <100 [see Paonita et al. 2013], are emitted. This, combined with the intermediate SO_2 fluxes observed especially since May 2023 (the May 2023 to June 2024 SO_2 flux average is 68 ± 26 tons/day), indicates that the sulfur output regime at La Fossa may have not completely recovered to background levels yet [see also Inguaggiato et al. 2023; Vita et al. 2023; Giuffrida et al. 2025]. It is important to keep in mind that volcanic systems often exhibit complex, non-linear behavior, and hence can stabilize at new baselines/states of monitored parameters without necessarily returning to prior conditions, e.g. at more evaluated sulfur degassing regime in the Vulcano case. The drivers for this higher-than-normal sulfur release [Inguaggiato et al. 2023] are still debated, but can potentially include a combination of (i) sulfur remobilization from hydrothermal minerals [Chiodini et al. 1993; Di Liberto et al. 2002], and (or) (ii) an increased supply of magmatic sulfur from mafic magma at depth b.s.l. (≥5 km) [Aiuppa et al. 2022; Giuffrida et al. 2025], perhaps combined with a reduced scrubbing of magmatic sulfur in the hydrothermal system, due to more rapid gas transit in the ascent conduit. Petrological evidence has found that multiple episodes of mafic magma resupply to the shallow magmatic system have taken places in the ~140-year temporal interval preceding the 1888–1890 La Fossa eruption [Giuffrida et al. 2025] and, although ground uplift (~7 cm) has been interpreted [Di Traglia et al. 2023] as caused by pressurization of a conduit-like gas feeding system within the shallow hydrothermal system [Chiarabba et al. 2004; Di Giuseppe et al. 2023], the fact this deformation is permanent (in spite of vanishing degassing activity at surface) leaves the possibility open that some (minor) reconfiguration of the plumbing system (e.g. the addition of small volume of magma at depth; Aiuppa et al. [2022] and Giuffrida et al. [2025]) may have taken place. As a complement to ongoing multi-parametric monitoring [Federico et al. 2023], periodic mapping of the fumarolic system may allow interpreting any further evolution of the unrest.

6 Conclusions

We have presented results of periodic gas surveys made at La Fossa cone on Vulcano Island, in which the spatial diversity of the summit fumarolic field was mapped and reconstructed over 2021 to 2024 using a portable Multi-GAS unit operated in walking traverse mode. Our results demonstrate a significant spatio-temporal evolution of the fumarolic field during the 2021–present degassing unrest. We have shown that the fumarolic field is broadly separated in two regions, separated by a NW–SE-trending boundary zone: (i) the crater rim area to the NE that has exhibited relatively uniform, intermediate CO_2/SO_2 ratio compositions (range, 19–31), and (ii) the inner crater fumaroles to the SW, that have exhibited wider temporal fluctuations, and overall dominance of more hydrothermal (CO_2/SO_2 ratios) gas signatures. This is interpreted as caused by oscillating phases of expansion and contraction of the gas chimney, centered underneath the 1888–1890 eruption outer carter rim (the cr6 crater rim of Di Traglia et al. [2013]), acting as the main transport structure of magmatic volatiles toward the surface. The intermediate, below-background CO_2/SO_2 ratios observed in crater rim area throughout 2021–2024, in conjunction with the higher-than-background SO_2 fluxes recorded, suggest that, despite the progressive vanishing of degassing activity since the acme of the unrest reached in fall 2021, hydrothermal activity conditions may stabilised at higher sulfur degassing levels than before the unrest.

Author Contributions

Simone Lentini: Writing—Original Draft, Visualization, Methodology, Investigation, Formal analysis, Data curation. Marcello Bitetto: Methodology, Investigation, Data curation. Luciano Curcio: Writing—Review & Editing, Methodology, Investigation, Data curation. Malte Seefeld: Visualization, Methodology, Investigation, Formal analysis. Angelo Vitale: Methodology, Investigation, Data curation. Piero Dellino: Supervision, Project administration, Funding acquisition. Roberto Sulpizio: Supervision, Project administration, Funding acquisition. Daniel Muller: Writing—Review & Editing, Methodology, Investigation, Data curation. Thomas R. Walter: Writing—Review & Editing, Methodology, Investigation. Alessandro Aiuppa: Writing—Original Draft, Investigation, Formal analysis, Data curation, Supervision, Project administration, Funding acquisition.

Acknowledgements

This study was carried out within the RETURN Extended Partnership and received funding from the European Union Next-GenerationEU (National Recovery and Resilience Plan – NRRP, Mission 4, Component 2, Investment 1.3 – D.D. 1243 2/8/2022, PE0000005. TRW was financially supported by ROTTnROCK, a research project funded by the European Research Council under the European Union's Horizon Europe Programme / ERC synergy grant n. [ERC-2023-SyG 101118491]. The manuscript benefited of constructive comments from two anonymous reviewers.

Data Availability

The data in csv format supporting the conclusions reached in this article (Relative DOI. 10.5281/zenodo.15298147) are available in a 7-Zip file at https://zenodo.org/records/15298147.

Copyright notice

References

Aiuppa, A., C. Federico, G. Giudice, and S. Gurrieri (2005). "Chemical mapping of a fumarolic field: La Fossa Crater, Vulcano Island (Aeolian Islands, Italy)". *Geophysical Research Letters* 32(13). DOI: 10.1029/2005gl023207.

Aiuppa, A., C. Federico, G. Giudice, S. Gurrieri, and M. Valenza (2006). "Hydrothermal buffering of the SO_2/H_2S ratio in volcanic gases: Evidence from La Fossa Crater fumarolic field, Vulcano Island". *Geophysical Research Letters* 33(21). DOI: 10.1029/2006gl027730.

Aiuppa, A., M. Bitetto, S. Calabrese, D. Delle Donne, J. Lages, F. P. La Monica, G. Chiodini, G. Tamburello, A. Cotterill, P. Fulignati, A. Gioncada, E. J. Liu, R. Moretti, and M. Pistolesi (2022). "Mafic magma feeds degassing unrest at Vulcano Island, Italy". *Communications Earth & Environment* 3(1). DOI: 10.1038/s43247-022-00589-1.

Aiuppa, A., M. Bitetto, D. Delle Donne, F. P. La Monica, G. Tamburello, D. Coppola, M. Della Schiava, L. Innocenti, G. Lacanna, M. Laiolo, F. Massimetti, M. Pistolesi, M. C. Silengo, and M. Ripepe (2021). "Volcanic CO_2 tracks the incubation period of basaltic paroxysms". *Science Advances* 7(38). DOI: 10.1126/sciadv.abh0191.

Aiuppa, A., T. P. Fischer, T. Plank, P. Robidoux, and R. Di Napoli (2017). "Along-arc, inter-arc and arc-to-arc variations in volcanic gas CO_2/S_T ratios reveal dual source of carbon in arc volcanism". *Earth-Science Reviews* 168, pages 24–47. DOI: 10.1016/j.earscirev.2017.03.005.

Aiuppa, A., R. Moretti, C. Federico, G. Giudice, S. Gurrieri, M. Liuzzo, P. Papale, H. Shinohara, and M. Valenza (2007). "Forecasting Etna eruptions by real-time observation of volcanic gas composition". *Geology* 35(12), page 1115. DOI: 10.1130/g24149a.1.

Aiuppa, A. and Y. Moussallam (2024). "Hydrogen and hydrogen sulphide in volcanic gases: abundance, processes, and atmospheric fluxes". *Comptes Rendus. Géoscience* 356(S1), pages 85–108. DOI: 10.5802/crgeos.235.

Alparone, S., A. Cannata, S. Gambino, S. Gresta, V. Milluzzo, and P. Montalto (2010). "Time-space variation of volcano-seismic events at La Fossa (Vulcano, Aeolian Islands, Italy): new insights into seismic sources in a hydrothermal system". *Bulletin of Volcanology* 72(7), pages 803–816. DOI: 10.1007/s00445-010-0367-6.

Barberi, F., G. Neri, M. Valenza, and L. Villari (1991). "1987–1990 unrest at Vulcano". *Journal of Volcanology and Geothermal Research* 1, pages 95–106.

Barde-Cabusson, S., A. Finizola, A. Revil, T. Ricci, S. Piscitelli, E. Rizzo, B. Angeletti, M. Balasco, L. Bennati, S. Byrdina, N. Carzaniga, A. Crespy, F. Di Gangi, J. Morin, A. Perrone, M. Rossi, E. Roulleau, B. Suski, and N. Villeneuve (2009). "New geological insights and structural control on fluid circulation in La Fossa cone (Vulcano, Aeolian Islands, Italy)". *Journal of Volcanology and Geothermal Research* 185(3), pages 231–245. DOI: 10.1016/j.jvolgeores.2009.06.002.

Buck, A. L. (1981). "New Equations for Computing Vapor Pressure and Enhancement Factor". *Journal of Applied Meteorology* 20(12), pages 1527–1532. DOI: 10.1175/1520-0450(1981)020<1527:nefcvp>2.0.co;2.

Campus, A., S. Aveni, M. Laiolo, F. Massimetti, and D. Coppola (2024). "Thermal unrest at La Fossa (Vulcano Island, Italy): the 2021–2023 VIIRS 375 m MIROVA-processed dataset". *Bulletin of Volcanology* 86(4). DOI: 10.1007/s00445-024-01721-z.

Cashman, K. V., R. S. J. Sparks, and J. D. Blundy (2017). "Vertically extensive and unstable magmatic systems: A unified view of igneous processes". *Science* 355(6331). DOI: 10.1126/science.aag3055.

Chiarabba, C., N. A. Pino, G. Ventura, and G. Vilardo (2004). "Structural features of the shallow plumbing system of Vulcano Island Italy". *Bulletin of Volcanology* 66(6), pages 477–484. DOI: 10.1007/s00445-003-0331-9.

Chiodini, G., R. Cioni, L. Marini, and C. Panichi (1995). "Origin of the fumarolic fluids of Vulcano Island, Italy and implications for volcanic surveillance". *Bulletin of Volcanology* 57(2), pages 99–110. DOI: 10.1007/bf00301400.

Chiodini, G., D. Granieri, R. Avino, S. Caliro, A. Costa, and C. Werner (2005). "Carbon dioxide diffuse degassing and estimation of heat release from volcanic and hydrothermal systems". *Journal of Geophysical Research: Solid Earth* 110(B8). DOI: 10.1029/2004jb003542.

Chiodini, G. (2009). "CO_2/CH_4 ratio in fumaroles a powerful tool to detect magma degassing episodes at quiescent volcanoes". *Geophysical Research Letters* 36(2). DOI: 10.1029/2008gl036347.

Chiodini, G., S. Caliro, P. De Martino, R. Avino, and F. Gherardi (2012). "Early signals of new volcanic unrest at Campi Flegrei caldera? Insights from geochemical data and physical simulations". *Geology* 40(10), pages 943–946. DOI: 10.1130/g33251.1.

Chiodini, G., S. Caliro, R. Avino, E. Bagnato, F. Capecchiacci, A. Carandente, C. Cardellini, C. Minopoli, G. Tamburello, S. Tripaldi, and A. Aiuppa (2022). "The Hydrothermal System of the Campi Flegrei Caldera, Italy". *Campi Flegrei*. Springer Berlin Heidelberg, pages 239–255. ISBN: 9783642370601. DOI: 10.1007/978-3-642-37060-1_9.

Chiodini, G., R. Cioni, and L. Marini (1993). "Reactions governing the chemistry of crater fumaroles from Vulcano Island, Italy, and implications for volcanic surveillance". *Applied Geochemistry* 8(4), pages 357–371. DOI: 10.1016/0883-2927(93)90004-z.

Chiodini, G. and L. Marini (1998). "Hydrothermal gas equilibria: the $H_2O-H_2-CO_2-CO-CH_4$ system". *Geochimica et Cosmochimica Acta* 62(15), pages 2673–2687. DOI: https://doi.org/10.1016/S0016-7037(98)00181-1.

Chiodini, G., A. Paonita, A. Aiuppa, A. Costa, S. Caliro, P. De Martino, V. Acocella, and J. Vandemeulebrouck (2016). "Magmas near the critical degassing pressure drive volcanic unrest towards a critical state". *Nature Communications* 7(1). DOI: 10.1038/ncomms13712.

Coppola, D., M. Laiolo, A. Campus, and F. Massimetti (2022). "Thermal unrest of a fumarolic field tracked using VIIRS imaging bands: The case of La fossa crater (Vulcano Island, Italy)". *Frontiers in Earth Science* 10. DOI: 10.3389/feart.2022.964372.

Darmawan, H., V. R. Troll, T. R. Walter, F. M. Deegan, H. Geiger, M. J. Heap, N. Seraphine, C. Harris, H. Humaida, and D. Müller (2022). "Hidden mechanical weaknesses within lava domes provided by buried high-porosity hydrothermal alteration zones". *Scientific Reports* 12(1). DOI: 10.1038/s41598-022-06765-9.

De Astis, G., F. Lucchi, P. Dellino, L. La Volpe, C. A. Tranne, M. L. Frezzotti, and A. Peccerillo (2013). "Chapter 11 Geology, volcanic history and petrology of Vulcano (central Aeolian archipelago)". *Geological Society, London, Memoirs* 37(1), pages 281–349. DOI: 10.1144/m37.11.

De Astis, G., D. M. Doronzo, and M. A. Di Vito (2023). "A review of the tectonic, volcanological and hazard history of Vulcano (Aeolian Islands, Italy)". *Terra Nova* 35(6), pages 471–487. DOI: 10.1111/ter.12678.

Delle Donne, D., A. Aiuppa, M. Bitetto, R. D'Aleo, M. Coltelli, D. Coppola, E. Pecora, M. Ripepe, and G. Tamburello (2019). "Changes in SO2 Flux Regime at Mt. Etna Captured by Automatically Processed Ultraviolet Camera Data". *Remote Sensing* 11(10). DOI: 10.3390/rs11101201.

Delle Donne, D., M. Ripepe, G. Lacanna, G. Tamburello, M. Bitetto, and A. Aiuppa (2016). "Gas mass derived by infrasound and UV cameras: Implications for mass flow rate". *Journal of Volcanology and Geothermal Research* 325, pages 169–178. DOI: 10.1016/j.jvolgeores.2016.06.015.

De Moor, J. M., C. Kern, G. Avard, C. Muller, A. Aiuppa, A. Saballos, M. Ibarra, P. LaFemina, M. Protti, and T. P. Fischer (2017). "A New Sulfur and Carbon Degassing Inventory for the Southern Central American Volcanic Arc: The Importance of Accurate Time-Series Data Sets and Possible Tectonic Processes Responsible for Temporal Variations in Arc-Scale Volatile Emissions". *Geochemistry, Geophysics, Geosystems* 18(12), pages 4437–4468. DOI: 10.1002/2017gc007141.

De Moor, J. M., A. Aiuppa, G. Avard, H. Wehrmann, N. Dunbar, C. Muller, G. Tamburello, G. Giudice, M. Liuzzo, R. Moretti, V. Conde, and B. Galle (2016). "Turmoil at Turrialba Volcano (Costa Rica): Degassing and eruptive processes inferred from high-frequency gas monitoring". *Journal of Geophysical Research: Solid Earth* 121(8), pages 5761–5775. DOI: 10.1002/2016jb013150.

Di Giuseppe, M. G., R. Isaia, and A. Troiano (2023). "Three-dimensional magnetotelluric modeling of Vulcano Island (Eolie, Italy) and its implications for understanding recent volcanic unrest". *Scientific Reports* 13(1). DOI: 10.1038/s41598-023-43828-x.

Di Liberto, V., P. Nuccio, and A. Paonita (2002). "Genesis of chlorine and sulphur in fumarolic emissions at Vulcano Island (Italy): assessment of pH and redox conditions in the hydrothermal system". *Journal of Volcanology and Geothermal Research* 116(1–2), pages 137–150. DOI: 10.1016/s0377-0273(02)00215-9.

Di Martino, R. M. R., S. Gurrieri, M. Camarda, G. Capasso, and V. Prano (2022). "Hazardous Changes in Soil CO_2 Emissions at Vulcano, Italy, in 2021". *Journal of Geophysical Research: Solid Earth* 127(11). DOI: 10.1029/2022jb024516.

Di Traglia, F., V. Bruno, F. Casu, O. Cocina, C. De Luca, F. Giudicepietro, G. Macedonio, M. Mattia, F. Monterroso, E. Privitera, and R. Lanari (2023). "Multi-Temporal InSAR, GNSS and Seismic Measurements Reveal the Origin of the 2021 Vulcano Island (Italy) Unrest". *Geophysical Research Letters* 50(24). DOI: 10.1029/2023gl104952.

Di Traglia, F., M. Pistolesi, M. Rosi, C. Bonadonna, R. Fusillo, and M. Roverato (2013). "Growth and erosion: The volcanic geology and morphological evolution of La Fossa (Island of Vulcano, Southern Italy) in the last 1000years". *Geomorphology* 194, pages 94–107. DOI: 10.1016/j.geomorph.2013.04.018.

Di Traglia, F., M. Pistolesi, C. Bonadonna, and M. Rosi (2024). "The last 1100 years of activity of La Fossa caldera, Vulcano Island (Italy): new insights into stratigraphy, chronology, and landscape evolution". *Bulletin of Volcanology* 86(5). DOI: 10.1007/s00445-024-01738-4.

Diliberto, I. S. (2013). "Time series analysis of high temperature fumaroles monitored on the island of Vulcano (Aeolian Archipelago, Italy)". *Journal of Volcanology and Geothermal Research* 264, pages 150–163. DOI: 10.1016/j.jvolgeores.2013.08.003.

– (2017). "Long-term monitoring on a closed-conduit volcano: A 25 year long time-series of temperatures recorded at La Fossa cone (Vulcano Island, Italy), ranging from 250 °C to 520 °C". *Journal of Volcanology and Geothermal Research* 346, pages 151–160. DOI: 10.1016/j.jvolgeores.2017.03.005.

Diliberto, I. S., L. Calderone, P. Cosenza, A. Mastrolia, and M. G. Di Figlia (2024). "The temperatures recorded from January 2020 to February 2023 in the diffuse degassing zone of the active cone of La Fossa Caldera". *Bulletin of Volcanology* 86(4). DOI: 10.1007/s00445-024-01730-y.

Edmonds, M., E. Liu, and K. Cashman (2022). "Open-vent volcanoes fuelled by depth-integrated magma degassing". *Bulletin of Volcanology* 84(3). DOI: 10.1007/s00445-021-01522-8.

Edmonds, M. and P. J. Wallace (2017). "Volatiles and Exsolved Vapor in Volcanic Systems". *Elements* 13(1), pages 29–34. DOI: 10.2113/gselements.13.1.29.

Federico, C., O. Cocina, S. Gambino, A. Paonita, S. Branca, M. Coltelli, F. Italiano, V. Bruno, T. Caltabiano, M. Camarda, G. Capasso, S. De Gregorio, I. S. Diliberto, R. M. R. Di Martino, S. Falsaperla, F. Greco, G. Pecoraino, G. Salerno, M. Sciotto, S. Bellomo, G. D. Grazia, F. Ferrari, A. Gattuso, L.

La Pica, M. Mattia, A. F. Pisciotta, L. Pruiti, and F. Sortino (2023). "Inferences on the 2021 Ongoing Volcanic Unrest at Vulcano Island (Italy) through a Comprehensive Multidisciplinary Surveillance Network". *Remote Sensing* 15(5), page 1405. DOI: 10.3390/rs15051405.

Fischer, T. P. and G. Chiodini (2015). "Volcanic, Magmatic and Hydrothermal Gases". *The Encyclopedia of Volcanoes*. Elsevier, pages 779–797. ISBN: 9780123859389. DOI: 10.1016/b978-0-12-385938-9.00045-6.

Frazzetta, G., P. Y. Gillot, L. Volpe, and M. F. Sheridan (1984). "Volcanic hazards at Fossa of Vulcano: Data from the last 6, 000 years". *Bulletin Volcanologique* 47(1), pages 105–124. DOI: 10.1007/bf01960543.

Fusillo, R., F. Di Traglia, A. Gioncada, M. Pistolesi, P. J. Wallace, and M. Rosi (2015). "Deciphering post-caldera volcanism: insight into the Vulcanello (Island of Vulcano, Southern Italy) eruptive activity based on geological and petrological constraints". *Bulletin of Volcanology* 77(9). DOI: 10.1007/s00445-015-0963-6.

Giggenbach, W. (1987). "Redox processes governing the chemistry of fumarolic gas discharges from White Island, New Zealand". *Applied Geochemistry* 2(2), pages 143–161. DOI: 10.1016/0883-2927(87)90030-8.

– (1997). "The origin and evolution of fluids in magmatic-hydrothermal systems". *Geochemistry of hydrothermal ore deposits*. Edited by H. L. Barnes. 3rd Edition. John Wiley & Sons, pages 737–796. ISBN: 047157144X.

Giuffrida, M., G. Salerno, and M. Viccaro (2025). "Multiple magma recharges over prolonged period ultimately trigger eruptions at Vulcano, Aeolian Islands". *Scientific Reports* 15(1). DOI: 10.1038/s41598-025-85496-z.

Harris, A. and A. Maciejewski (2000). "Thermal surveys of the Vulcano Fossa fumarole field 1994–1999: evidence for fumarole migration and sealing". *Journal of Volcanology and Geothermal Research* 102(1–2), pages 119–147. DOI: 10.1016/s0377-0273(00)00184-0.

Harris, A., S. Alparone, A. Bonforte, J. Dehn, S. Gambino, L. Lodato, and L. Spampinato (2012). "Vent temperature trends at the Vulcano Fossa fumarole field: the role of permeability". *Bulletin of Volcanology* 74(6), pages 1293–1311. DOI: 10.1007/s00445-012-0593-1.

Harris, A. J. L., L. Lodato, J. Dehn, and L. Spampinato (2009). "Thermal characterization of the Vulcano fumarole field". *Bulletin of Volcanology* 71(4), pages 441–458. DOI: 10.1007/s00445-008-0236-8.

Henley, R. W. and T. P. Fischer (2021). "Sulfur sequestration and redox equilibria in volcanic gases". *Journal of Volcanology and Geothermal Research* 414, page 107181. DOI: 10.1016/j.jvolgeores.2021.107181.

Holohan, E. P., B. van Wyk de Vries, and V. R. Troll (2008). "Analogue models of caldera collapse in strike-slip tectonic regimes". *Bulletin of Volcanology* 70(7), pages 773–796. DOI: 10.1007/s00445-007-0166-x.

Inguaggiato, S., L. Calderone, C. Inguaggiato, A. Mazot, S. Morici, and F. Vita (2012). "Long-time variation of soil CO_2 fluxes at the summit crater of Vulcano (Italy)". *Bulletin of Volcanology* 74(8), pages 1859–1863. DOI: 10.1007/s00445-012-0637-6.

Inguaggiato, S., I. S. Diliberto, C. Federico, A. Paonita, and F. Vita (2018). "Review of the evolution of geochemical monitoring, networks and methodologies applied to the volcanoes of the Aeolian Arc (Italy)". *Earth-Science Reviews* 176, pages 241–276. DOI: 10.1016/j.earscirev.2017.09.006.

Inguaggiato, S., M. Liotta, D. Rouwet, F. Tassi, F. Vita, B. Schiavo, S. Ono, and N. S. Keller (2023). "Sulfur origin and flux variations in fumarolic fluids of Vulcano Island, Italy". *Frontiers in Earth Science* 11. DOI: 10.3389/feart.2023.1197796.

Inguaggiato, S., F. Vita, I. S. Diliberto, C. Inguaggiato, A. Mazot, M. Cangemi, and M. Corrao (2022). "The volcanic activity changes occurred in the 2021–2022 at Vulcano island (Italy), inferred by the abrupt variations of soil CO_2 output". *Scientific Reports* 12(1). DOI: 10.1038/s41598-022-25435-4.

INGV monitoring reports. URL: https://www.ct.ingv.it/index.php/monitoraggio-e-sorveglianza/prodotti-del-monitoraggio/bollettini-settimanali-multidisciplinari.

Italiano, F., G. Pecoraino, and P. M. Nuccio (1998). "Steam output from fumaroles of an active volcano: Tectonic and magmatic-hydrothermal controls on the degassing system at Vulcano (Aeolian arc)". *Journal of Geophysical Research: Solid Earth* 103(B12), pages 29829–29842. DOI: 10.1029/98jb02237.

Keller, J. (1980). "The island of Vulcano". *Rendiconti Società Italiana di Mineralogia e Petrologia* 1, pages 369–414.

Kereszturi, G., M. Heap, L. N. Schaefer, H. Darmawan, F. M. Deegan, B. Kennedy, J.-C. Komorowski, S. Mead, M. Rosas-Carbajal, A. Ryan, V. R. Troll, M. Villeneuve, and T. R. Walter (2023). "Porosity, strength, and alteration – Towards a new volcano stability assessment tool using VNIR-SWIR reflectance spectroscopy". *Earth and Planetary Science Letters* 602, page 117929. DOI: 10.1016/j.epsl.2022.117929.

Kern, C., F. Kick, P. Lübcke, L. Vogel, M. Wöhrbach, and U. Platt (2010). "Theoretical description of functionality, applications, and limitations of SO_2 cameras for the remote sensing of volcanic plumes". *Atmospheric Measurement Techniques* 3(3), pages 733–749. DOI: 10.5194/amt-3-733-2010.

Kern, C., A. Aiuppa, and J. M. de Moor (2022). "A golden era for volcanic gas geochemistry?" *Bulletin of Volcanology* 84(5). DOI: 10.1007/s00445-022-01556-6.

Lo Bue Trisciuzzi, G., A. Aiuppa, G. Salerno, M. Bitetto, L. Curcio, L. Innocenti, G. Lacanna, J. P. Nogueira Lages, F. M. Lo Forte, S. R. Maugeri, F. Murè, P. Principato, M. Ripepe, A. Vitale, and D. Delle Donne (2024). "Improved volcanic SO2 flux records from integrated scanning-DOAS and UV Camera observations." *Journal of Volcanology and Geothermal Research* 455, page 108207. DOI: 10.1016/j.jvolgeores.2024.108207.

Madonia, P., M. Cangemi, M. Costa, and I. Madonia (2016). "Mapping fumarolic fields in volcanic areas: A methodological approach based on the case study of La Fossa cone, Vulcano island (Italy)". *Journal of Volcanology and Geothermal Research* 324, pages 1–7. DOI: 10.1016/j.jvolgeores.2016.05.014.

Malaguti, A. B., M. Rosi, M. Pistolesi, F. Speranza, and M. Menzies (2021). "The contribution of palaeomagnetism, tephrochronology and radiocarbon dating to refine the last 1100 years of eruptive activity at Vulcano (Italy)". *Bulletin of Volcanology* 84(1). DOI: 10.1007/s00445-021-01515-7.

Mannini, S., A. J. L. Harris, D. E. Jessop, M. O. Chevrel, and M. S. Ramsey (2019). "Combining Ground- and ASTER-Based Thermal Measurements to Constrain Fumarole Field Heat Budgets: The Case of Vulcano Fossa 2000–2019". *Geophysical Research Letters* 46(21), pages 11868–11877. DOI: 10.1029/2019gl084013.

Mantovani, E., M. Viti, D. Babbucci, and C. Tamburelli (2023). "Generation of the Quaternary Normal Faults in the Messina Strait (Italy)". *Geosciences* 13(8), page 248. DOI: 10.3390/geosciences13080248.

Marini, L., C. Principe, and M. Lelli (2022). "The Magmatic–Hydrothermal System Hosted in the Campi Flegrei Caldera with Emphasis on the Solfatara". *The Solfatara Magmatic-Hydrothermal System*. Springer International Publishing, pages 23–61. ISBN: 9783030984717. DOI: 10.1007/978-3-030-98471-7_3.

Mercalli, G. and O. Silvestri (1891). "Le eruzioni dell'isola di Vulcano, incominciate il 3 Agosto 1888 e terminate il 22 Marzo 1890". *Relazione scientifica 1891: Annuo Ufficio Centrale Meteorologia e Geodinamica* 10(4), pages 1–213.

Müller, D., S. Bredemeyer, E. Zorn, E. De Paolo, and T. R. Walter (2021). "Surveying fumarole sites and hydrothermal alteration by unoccupied aircraft systems (UAS) at the La Fossa cone, Vulcano Island (Italy)". *Journal of Volcanology and Geothermal Research* 413, page 107208. DOI: 10.1016/j.jvolgeores.2021.107208.

Müller, D., T. R. Walter, V. R. Troll, J. Stammeier, A. Karlsson, E. de Paolo, A. F. Pisciotta, M. Zimmer, and B. De Jarnatt (2024). "Anatomy of a fumarole field: drone remote-sensing and petrological approaches reveal the degassing and alteration structure at La Fossa cone, Vulcano, Italy". *Solid Earth* 15(9), pages 1155–1184. DOI: 10.5194/se-15-1155-2024.

Norton, D. L. (1984). "Theory of Hydrothermal Systems". *Annual Review of Earth and Planetary Sciences* 12(1), pages 155–177. DOI: 10.1146/annurev.ea.12.050184.001103.

Nuccio, P., A. Paonita, and F. Sortino (1999). "Geochemical modeling of mixing between magmatic and hydrothermal gases: the case of Vulcano Island, Italy". *Earth and Planetary Science Letters* 167(3–4), pages 321–333. DOI: 10.1016/s0012-821x(99)00037-0.

Nuccio, P. and A. Paonita (2001). "Magmatic degassing of multicomponent vapors and assessment of magma depth: application to Vulcano Island (Italy)". *Earth and Planetary Science Letters* 193(3–4), pages 467–481. DOI: 10.1016/s0012-821x(01)00512-x.

Oppenheimer, C., T. Fischer, and B. Scaillet (2014). "Volcanic Degassing: Process and Impact". *Treatise on Geochemistry*. Elsevier, pages 111–179. ISBN: 9780080983004. DOI: 10.1016/b978-0-08-095975-7.00304-1.

Pailot-Bonnétat, S., V. Rafflin, A. Harris, I. S. Diliberto, G. Ganci, G. Bilotta, A. Cappello, G. Boudoire, F. Grassa, A. Gattuso, and M. Ramsey (2023). "Anatomy of thermal unrest at a hydrothermal system: case study of the 2021–2022 crisis at Vulcano". *Earth, Planets and Space* 75(1). DOI: 10.1186/s40623-023-01913-5.

Paonita, A., R. Favara, P. Nuccio, and F. Sortino (2002). "Genesis of fumarolic emissions as inferred by isotope mass balances: CO 2 and water at Vulcano Island, Italy". *Geochimica et Cosmochimica Acta* 66(5), pages 759–772. DOI: 10.1016/s0016-7037(01)00814-6.

Paonita, A., C. Federico, P. Bonfanti, G. Capasso, S. Inguaggiato, F. Italiano, P. Madonia, G. Pecoraino, and F. Sortino (2013). "The episodic and abrupt geochemical changes at La Fossa fumaroles (Vulcano Island, Italy) and related constraints on the dynamics, structure, and compositions of the magmatic system". *Geochimica et Cosmochimica Acta* 120, pages 158–178. DOI: 10.1016/j.gca.2013.06.015.

Peccerillo, A. (2017). *Cenozoic Volcanism in the Tyrrhenian Sea Region*. Springer International Publishing. ISBN: 9783319424910. DOI: 10.1007/978-3-319-42491-0.

Phillipson, G., R. Sobradelo, and J. Gottsmann (2013). "Global volcanic unrest in the 21st century: An analysis of the first decade". *Journal of Volcanology and Geothermal Research* 264, pages 183–196. DOI: 10.1016/j.jvolgeores.2013.08.004.

Revil, A., A. Finizola, S. Piscitelli, E. Rizzo, T. Ricci, A. Crespy, B. Angeletti, M. Balasco, S. Barde Cabusson, L. Bennati, A. Bolève, S. Byrdina, N. Carzaniga, F. Di Gangi, J. Morin, A. Perrone, M. Rossi, E. Roulleau, and B. Suski (2008). "Inner structure of La Fossa di Vulcano (Vulcano Island, southern Tyrrhenian Sea, Italy) revealed by high-resolution electric resistivity tomography coupled with self-potential, temperature, and CO_2 diffuse degassing measurements". *Journal of Geophysical Research: Solid Earth* 113(B7). DOI: 10.1029/2007jb005394.

Revil, A., T. C. Johnson, and A. Finizola (2010). "Three-dimensional resistivity tomography of Vulcan's forge, Vulcano Island, southern Italy". *Geophysical Research Letters* 37(15). DOI: 10.1029/2010gl043983.

Rosi, M., V. Acocella, R. Cioni, F. Bianco, A. Costa, P. De Martino, G. Giordano, and S. Inguaggiato (2022). "Defining the Pre-Eruptive States of Active Volcanoes for Improving Eruption Forecasting". *Frontiers in Earth Science* 10. DOI: 10.3389/feart.2022.795700.

Rosi, M., F. Di Traglia, M. Pistolesi, T. Esposti Ongaro, M. de'Michieli Vitturi, and C. Bonadonna (2018). "Dynamics of shallow hydrothermal eruptions: new insights from Vulcano's Breccia di Commenda eruption". *Bulletin of Volcanology* 80(12). DOI: 10.1007/s00445-018-1252-y.

Ruch, J., L. Vezzoli, R. De Rosa, R. Di Lorenzo, and V. Acocella (2016). "Magmatic control along a strike-slip volcanic arc: The central Aeolian arc (Italy): MAGMATISM AND STRIKE-SLIP FAULTING". *Tectonics* 35(2), pages 407–424. DOI: 10.1002/2015tc004060.

Selva, J., C. Bonadonna, S. Branca, G. De Astis, S. Gambino, A. Paonita, M. Pistolesi, T. Ricci, R. Sulpizio, A. Tibaldi, and A. Ricciardi (2020). "Multiple hazards and paths to eruptions: A review of the volcanic system of Vulcano (Aeolian Islands, Italy)". *Earth-Science Reviews* 207, page 103186. DOI: 10.1016/j.earscirev.2020.103186.

Shinohara, H. (2005). "A new technique to estimate volcanic gas composition: plume measurements with a portable multi-sensor system". *Journal of Volcanology and Geothermal Research* 143(4), pages 319–333. DOI: 10.1016/j.jvolgeores.2004.12.004.

Soligo, M., G. De Astis, M. C. Delitala, L. La Volpe, A. Taddeucci, and P. Tuccimei (2000). "Uranium-series disequilibria in the products from Vulcano Island (Sicily, Italy): isotopic chronology and magmatological implications". *Acta Vulcanologica* 12(1/2), pages 49–62.

Stix, J. and J. M. de Moor (2018). "Understanding and forecasting phreatic eruptions driven by magmatic degassing". *Earth, Planets and Space* 70(1). DOI: 10.1186/s40623-018-0855-z.

Stumpp, D., I. Cabrera-Pérez, G. Savard, T. Ricci, S. Alparone, A. Ursino, M. Palano, F. Sparacino, F. Munoz-Burbano, C. Barat, M.-P. R. Hardy, J. Ruch, C. Bonadonna, and M. Lupi (2024). "Imaging volcanoes during unrest: Ambient Noise Tomography of a transient plumbing system, Vulcano, Italy." DOI: 10.21203/rs.3.rs-4767509/v1.

Symonds, R., T. Gerlach, and M. Reed (2001). "Magmatic gas scrubbing: implications for volcano monitoring". *Journal of Volcanology and Geothermal Research* 108(1–4), pages 303–341. DOI: 10.1016/s0377-0273(00)00292-4.

Symonds, R. B., W. I. Rose, G. J. S. Bluth, and T. M. Gerlach (1994). "Volcanic-gas studies: methods, results, and applications". *Volatiles in Magmas*. Edited by M. R. Carroll and J. R. Holloway. Berlin, Boston: De Gruyter, pages 1–66. ISBN: 9781501509674. DOI: 10.1515/9781501509674-007.

Vaselli, O., F. Tassi, E. Duarte, E. Fernandez, R. J. Poreda, and A. D. Huertas (2010). "Evolution of fluid geochemistry at the Turrialba volcano (Costa Rica) from 1998 to 2008". *Bulletin of Volcanology* 72(4), pages 397–410. DOI: 10.1007/s00445-009-0332-4.

Vergniolle, S. and N. Métrich (2022). "An interpretative view of open-vent volcanoes". *Bulletin of Volcanology* 84(9). DOI: 10.1007/s00445-022-01581-5.

Vita, F., B. Schiavo, C. Inguaggiato, S. Inguaggiato, and A. Mazot (2023). "Environmental and Volcanic Implications of Volatile Output in the Atmosphere of Vulcano Island Detected Using SO_2 Plume (2021–23)". *Remote Sensing* 15(12), page 3086. DOI: 10.3390/rs15123086.